

Politecnico di Torino

Master's Degree in Biomedical Engineering



Master's Thesis

3D printing of molecularly imprinted polymers for removal of antibiotics from aqueous solutions

Supervisor:
Dott. Ignazio Roppolo

Candidate:
Sara Vallero

Co-supervisor:
Dott. Simone Marasso

A.Y. 2023/2024

Sommario

Abstract	5
1. Molecularly Imprinted Polymers (MIPs): introduction, context and purpose.....	6
1.1 MIPs formulation: role and effects of individual ingredients.....	10
1.1.1 Template Molecule	10
1.1.2 Functional Monomer	11
1.1.3. Cross-Linker.....	13
1.1.4. Solvent.....	14
1.1.5. Initiator of Polymerization	15
1.2. Manufacture of MIPs: traditional and innovative methodologies	17
1.2.1. Strategies for the synthesis of Molecularly Imprinted Polymers	17
1.2.2. Methods of synthesizing MIPs.....	18
1.3. Use of MIPs: debinding to rebinding procedure	24
1.3.1. General overview of template removal.....	24
1.3.2. General overview of analyte binding	29
2. VAT 3D printing	32
2.1. Fundamentals of photopolymerization.....	32
2.2. Polymeric 3D printing: background and technologies	33
2.3. 3D printing methods	36
2.4. VAT 3D printing.....	36
2.4.1. Laser-SLA.....	37
2.4.2. Digital Light Processing (DLP)	38
2.5. 3D printing of MIP	39
3. Materials and Methods.....	41
3.1 Ingredients of the Formulation	41
3.1.1. Molecule Template	41
3.1.2. Functional Monomer.....	42
3.1.3. Crosslinker	42
3.1.4. Solvent.....	43
3.1.5. Photoinitiator.....	44
3.2. Preparation of the Formulation.....	44
3.2.1. MIP resin: Molecularly Imprinted Polymer	44
3.2.2. NIP resin: Non-Imprinted Polymer	45
3.3. DLP 3D Printing	46
3.3.1. DLP 3D Printer	46
3.3.2. Printing Process, Cleaning and Post-Curing	47

3.4.	Debinding, rebinding, washing after rebinding process	48
3.4.1.	Debinding o washing: washing conditions.....	48
3.4.2.	Rebinding process: features of the rebinding experiment.....	48
3.4.3.	Washing after rebinding process.....	49
3.5.	Characterization Methods	49
3.5.1.	Rheology	50
3.5.2.	Photo Rheology	50
3.5.3.	UV/visible spectroscopy.....	52
3.5.4.	Calibration Curve.....	55
3.5.5.	FTIR Spectroscopy in Attenuated Total Reflectance (FT-IR ATR)	56
3.5.6.	Atomic Force Microscope (AFM)	57
3.5.7.	3D Scanner	58
4.	Samples printing and results analysis.....	59
4.1.	Formulation's preparation and characterization.....	59
4.1.1.	Formulation's preparation	59
4.1.2.	Formulation's characterization	60
4.2.	3D printing process optimization and characterization	62
4.2.1.	CAD geometry	62
4.2.2.	Printing process and parameter optimisation	63
4.2.3.	Printed samples' characterization	67
4.3.	Debinding	69
4.4.	Rebinding experiments	73
4.4.1.	OTC calibration curve.....	73
4.4.2.	Stability test of the rebinding solution	75
4.4.3.	First experiment, DOT1: MIP and NIP	76
4.4.4.	Second experiment, DOT2: MIP and NIP	77
4.4.5.	Third experiment, DOT3: MIP and NIP	79
4.4.6.	Fourth and fifth experiment: gyroids 1 MIP	81
4.4.7.	Sixth experiment: comparison of different surface area on MIP gyroids	84
4.5.	Washing After Rebinding (WAR).....	85
5.	Conclusions and future work.....	87
	Bibliography	89

Abstract

The growing prevalence of antibiotics in water constitutes a severe environmental and health risk, necessitating novel methods development. This thesis investigates the use of 3D printed Molecularly Imprinted Polymers (MIPs), which are particularly designed to adsorb antibiotics from aqueous solutions. MIPs are artificial receptors created using molecular imprinting technology, which includes producing holes shaped like a specific template inside a polymer matrix. MIPs exhibit selectivity and specificity for a predefined analyte employed in the imprinting process, replicating the natural molecular recognition mechanism seen in biological receptors. In addition, MIPs have various benefits over biological receptors, including increased robustness and physical resistance, endurance to high temperatures and pressures, cheaper cost, simplicity of manufacture, and diversity in template selection.

MIPs typically consist of target molecule that acts as the template, that interacts with a functional monomer, a cross-linker that forms the polymer matrix, and an initiator that induces the polymerization reaction.

This thesis focuses on the use of 3D printing to produce MIPs, with Digital Light Processing (DLP) technology, which allows to produce complex and self-supporting 3D structures.

After testing the materials' capacity to operate as MIPs by printing basic dots and utilizing UV-Visible spectroscopy, more complicated designs were investigated. The accuracy of the printing technique and its ability to capture template molecules were also studied. This removal technique provides a viable alternative for treating antibiotic-contaminated water and marks a big step forward in the development of more efficient and sustainable water purification systems.

1. Molecularly Imprinted Polymers (MIPs): introduction, context and purpose

The quality of food and water suitable for human consumption is a pressing global concern, underscoring the need for effective filtration systems to fight micropollutants. These substances, including industrial chemicals, pharmaceuticals, antibiotics, pesticides, and emerging contaminants, even in minute quantities, pose significant threats to human health and to environment. They persist in trace amounts in various environmental settings, accumulating in food and water sources. This persistence leads to widespread implications for human safety worldwide. [1], [2]

Micropollutants originate from different sources such as urban, agricultural, and industrial discharges, and their presence exacerbates risks to human health by disrupting the endocrine system and contributing to chronic health issues. In agricultural contexts, these pollutants can infiltrate the food chain, introducing harmful substances into the human diet. [3]

Particular concerns are related to the antibiotic contamination, driven by the unregulated use of these drugs in human, veterinary, and agricultural sectors. This has resulted in their accumulation in the environment, fostering the development and spread of antibiotic-resistant bacteria. This phenomenon, called antimicrobial resistance, is a critical public health challenge, compromising the efficacy of antibiotic treatments and increasing the prevalence of hard-to-treat infections. Research [4] indicates that elevated levels of these antibiotics have adverse effects on the development, reproduction, and behaviour of aquatic species, including fish, invertebrates, and algae, potentially altering biodiversity and ecological dynamics in aquatic environments. [4]

One suggested solution to address this problem is the removal of antibiotics from wastewater before they can reach natural water or food chain.[3] However, current filtration systems like nano-filtration; bioremediation; chemical sedimentation; coagulation; and oxidation [5] are not always effective for the sufficient removal of trace concentrations of organic compounds. They have many limitations in terms of filtering efficiency and the costs incurred to carry out the entire process. Therefore, it is essential to research and develop new technologies for this purpose that are both

effective and economically advantageous to effectively protect public health and the environment.[6]

In this context, an innovative and effective strategy for recognizing specific molecules within solutions is molecular sensing. [7] This is a sophisticated technology that allows the detection and quantification of specific molecules in a sample. To find target molecules with great precision and sensitivity, this process uses a variety of physical and chemical methods. Molecular sensing employs sensors designed to recognize and respond to molecules or groups of molecules, these sensors rely on various principles, such as physical, chemical, or biological interactions between the sensor and the target molecule. Molecular sensors are often used in a wide range of applications, particularly in environmental monitoring, food safety, medical diagnostics, and biotechnology.

Examining molecular sensing through chemical recognition methods reveals the existence of highly specific sensors that emulate receptor-ligand interactions. Here, a receptor—a molecule or material with a binding cavity—interacts with a ligand, the specific molecule targeted for identification by the receptor. The interaction between the ligand and the receptor is exceptionally precise, primarily relying on non-covalent interactions like hydrogen bonds, van der Waals forces, ionic interactions, and hydrophobic interactions.

A specific example of molecular sensing with chemical recognition methods is represented by Molecularly Imprinted Polymers (MIPs), which are the subject of this thesis.

MIPs are synthetic receptors designed to recognize specific molecular shapes, exemplifying the application of molecular recognition in polymer systems. [8], [9] They can determine absolute configuration and quantifying enantiomeric excess. Moreover, MIPs can be engineered to respond to external stimuli, such as temperature, thereby enabling controlled molecular recognition.[8], [9]

These polymers are created through Molecular Imprinting Technology (MIT), which involves creating polymers with specific binding sites that are complementary to a target molecule, also known as the "template." [10] The process of creating "molecular

imprints" in polymers allows highly specific recognition and selectivity for the target molecule.

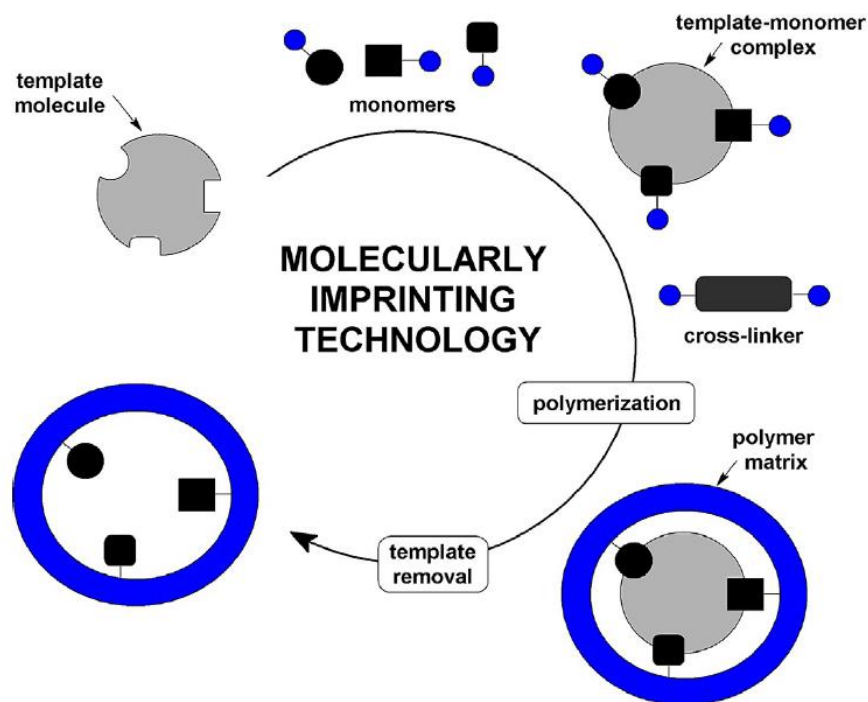


Fig. 1 Scheme of Molecular Imprinting process.[11]

The early discoveries by Polyakov, Pauling, Wulff, and Mosbach laid the foundations for the development of MIPs.[12] Today, Molecular Imprinting Technology (MIT) is widely employed across different fields, providing innovative solutions for specific molecule [13] recognition and removal in various contexts. MIT represents a synthetic approach to developing robust molecular recognition materials that emulate natural entities such as antibodies and biological receptors. This area of research is essential, positioning molecular imprinting as a leading strategy for creating materials capable of recognition comparable to natural systems. [8] MIT is noticed for its versatility and promise in recognizing both biological and chemical entities, encompassing amino acids, proteins, nucleotide derivatives, pollutants, drugs, and food components. Applications span separation sciences, chemical sensors, catalysis, drug delivery, and biological receptor systems. [8]

The technology that supports the creation of MIPs involves the formation of a complex between an analyte (template) and a functional monomer. Following polymerization in the presence of a cross-linking agent, a three-dimensional polymer network is

established. Post-polymerization, the template is extracted from the polymer, leaving behind specific recognition sites that mirror the shape, size, and chemical functionality of the template molecule. Intermolecular interactions such as hydrogen bonds, dipole-dipole, and ionic interactions guide the molecular rebinding process, enabling the polymer to selectively bind the template molecules. [15]

In summary, MIT enables the creation of artificial receptors that exhibit selectivity and specificity towards particular analytes. Molecularly Imprinted Polymers offer significant advantages such as high selectivity and affinity for target molecules used during imprinting. Compared to natural biological systems, MIPs boast enhanced physical durability, resistance to extreme conditions, and stability against various chemical environments. They are also cost-effective to produce and maintain their recognition capabilities over extended periods at room temperature, making them practical for long-term applications. [16]

Considering the present circumstances and the problem targeted by this thesis project, the work will focus on the creation of MIPs using additive manufacturing techniques through DLP (Digital Light Processing) 3D printing technology. This is a new manufacturing methodology, in fact 3D printing of MIPs is still barely studied in the literature, but offers an innovative, promising, and scalable approach to produce these synthetic receptors.

The objective of this thesis is to develop and optimize a 3D printing methodology to make MIPs specifically designed for the efficient removal of Oxytetracycline antibiotic from contaminated solutions. Through a complete analysis of the printing parameters and the absorption characteristics of the MIPs, this research aims to contribute to the development of sustainable and effective solutions for the removal of contaminants. This will help reduce pharmaceutical pollution and improve the quality of water resources, the environment, and consumer products.

1.1 MIPs formulation: role and effects of individual ingredients

As previously mentioned, Molecularly Imprinted Polymers (MIPs) are synthetic materials designed to have specific binding sites for a particular target molecule.[15] Molecularly Imprinted Polymers (MIPs) consist of various key components and the synthesis process of these materials can be summarized in three main steps:

- **Formation of the pre-polymerization complex:** The functional groups of the functional monomer strongly bind to those of the template molecule to create the complex. Essentially, the monomer is built around the template after sufficient mixing. A solvent may be used in this step to facilitate the dissolution and binding of the other two components.
- **Polymerization process:** The crosslinker and a polymerization initiator are introduced into the mixture; the crosslinker polymerizes and creates a three-dimensional polymer matrix around the pre-polymerization complex through heating or UV light.
- **Washing or debinding:** This final step involves the removal of the template, to obtain a polymer with specific recognition sites in the matrix that are comparable in shape, size, and chemical activity to the template molecule that enable its specific binding.

Below, the main components of MIPs will be examined in detail, along with their effects and purposes within the formation of these polymers.

1.1.1 Template Molecule

The first essential ingredient for the creation of MIPs is the template molecule. This is the target molecule that is first imprinted into the polymer and later recognized.

The primary role of the template is to direct the formation of specific recognition sites and guide the spatial orientation of the functional monomers during polymer formation. This orientation creates a highly specific three-dimensional recognition

environment. Additionally, the template must not contain groups that inhibit polymerization, ensuring that during the polymerization process, it contributes to the stability of the reaction and ensures that the monomers and cross-linker form a robust cross-linked structure around it.

The interactions that are created during synthesis, between template and other polymer components define the specificity of the binding site. These are influenced by the characteristics of the template molecule, so it is important to choose this compound accurately. [16]

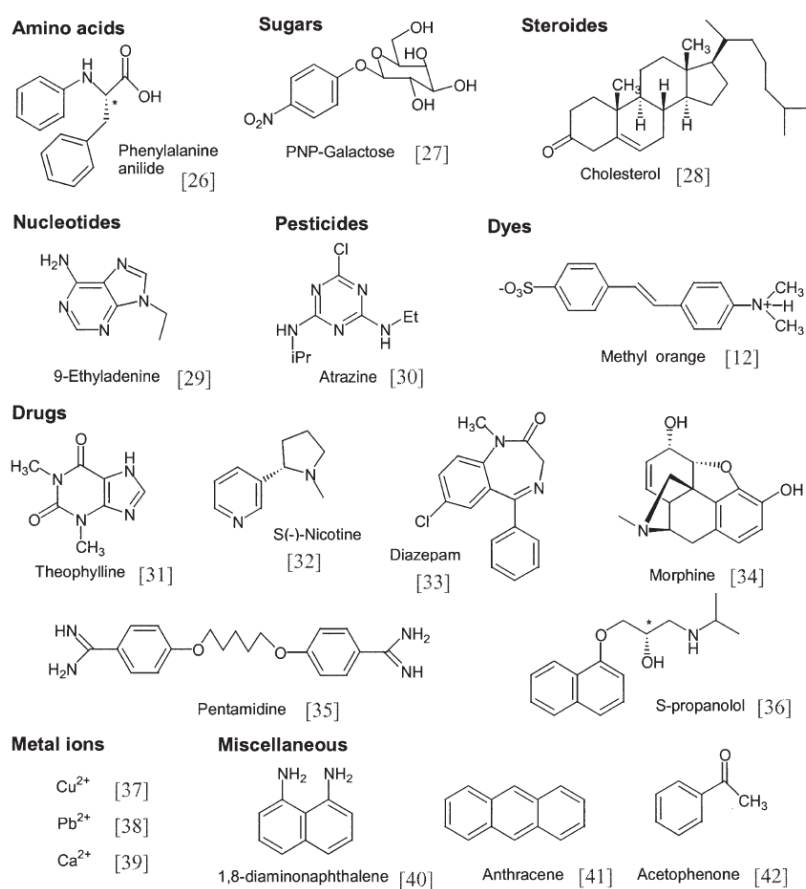


Fig. 2 Some examples of compounds used as template molecule in MIPs formulation.[16]

1.1.2 Functional Monomer

The functional monomer directly interacts with the template molecule, orienting itself around it to form cavities that are complementary, once polymerized and cross-linked, to the template in terms of shape and exposed functional groups. Moreover, it helps maintain the integrity of these recognition cavities after the template is removed,

ensuring the stability and robustness of the MIP to withstand adverse conditions, thus providing a long shelf life. The functional monomers' chemical nature (e.g., acids, bases, hydrophobic, or hydrophilic groups) influences the MIP's specificity and affinity. So, a critical step in MIP synthesis is identifying a suitable functional monomer that can form selective antibody-antigen or donor-acceptor complexes and has strong interactions with the template.

The stoichiometric ratio of template to functional monomer is crucial; in covalent imprinting, it is controlled by the template, while in non-covalent imprinting, it's provided in larger quantities than the template [17], [20]. Applying Le Chatelier's principle [18], increasing the binding capacity or constituent concentration in the pre-polymer complex enhances the binding cavities, thus improving the polymer's selectivity. Matching the functionalities of the template molecule and the functional monomer, such as pairing H-bond donors with H-bond acceptors, maximizes the formation of the pre-polymerization complex and the imprinting effect. [19]

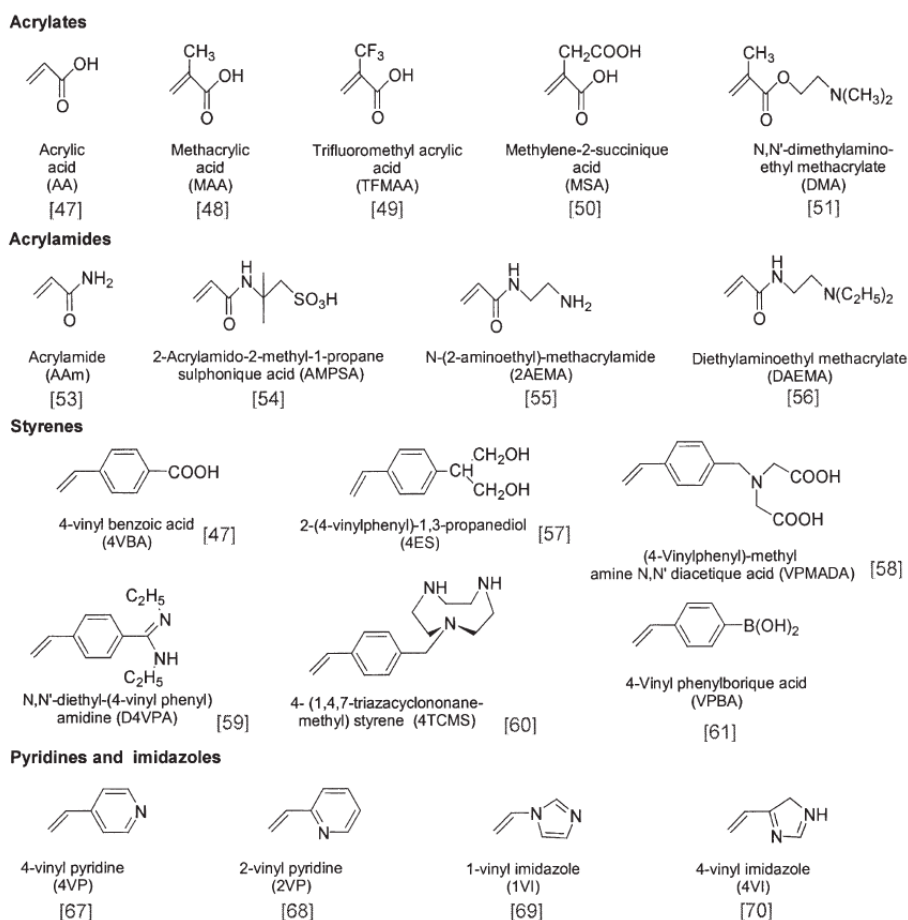


Fig. 3 The monomers most used in MIP's fabrication.[16]

1.1.3. Cross-Linker

The cross-linker is a crucial component that forms a three-dimensional network structure around the template-monomer complex, providing mechanical and chemical stability to the resulting polymer. This cross-linking agent reacts with the functional monomers and with itself during polymerization to create covalent bonds, forming a solid network that encapsulates the template-monomer complex.[5]

The cross-linker provides the stiffness to maintain functional cavities, reduces imprinted site deformation and makes it more durable to temperature variations, high pressures compared to a linear polymer.[10]

Some research,[20], [24] investigate how the degree of crosslinking affects MIP selectivity. The data also include the study's findings, such as a comparison of three distinct crosslinkers and their amounts. The needed amount of crosslinking is often above 70%.

Various studies [20], [24] have also found that in networks based on non-covalent interactions, only around 10% of the created sites are active.

In conclusion, the choice of the cross-linker depends on the desired properties of the final MIP, including rigidity, porosity, and compatibility with the functional monomers and the template molecule.

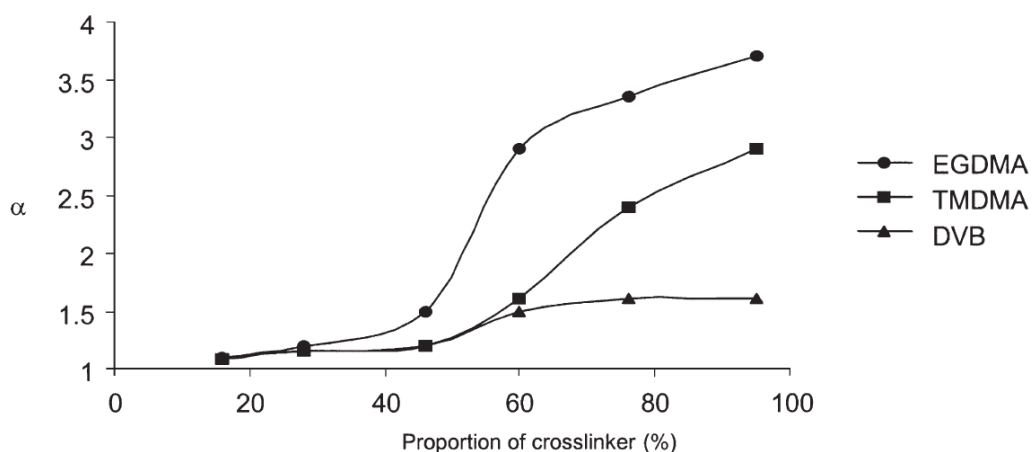


Fig. 4 Influence of the proportion of crosslinker on the recognition specificity of MIPs.[16], [21]

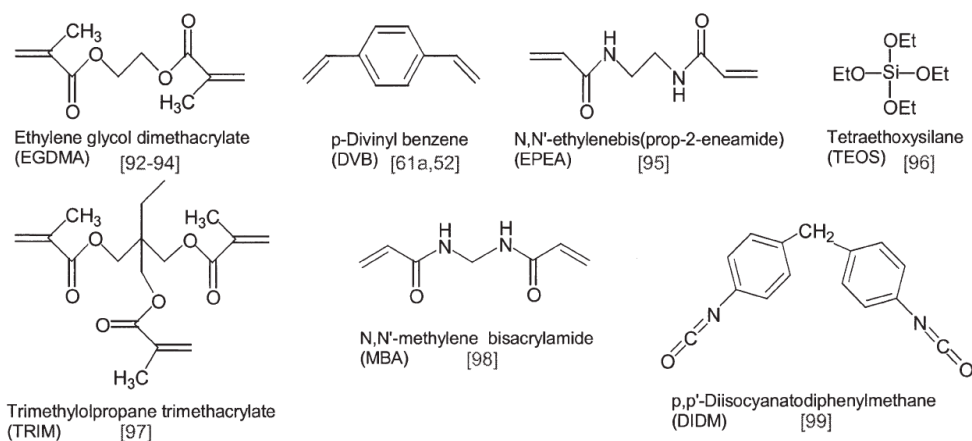


Fig. 4 The most used crosslinkers in MIP's fabrication.[16]

1.1.4. Solvent

The primary role of the solvent, is to dissolve the template and monomer, facilitating the formation of the pre-polymerization complex. It guarantees a homogeneous distribution of all components in the final mixture, preventing the formation of aggregates during polymerization.

Additionally, the solvent does not actively participate in the polymerization reaction but can influence the non-covalent interactions between the template molecule and the functional monomers. For example, polar protic, aprotic, and non-polar solvents can modulate these interactions, determining the efficiency with which the template directs the organization of the functional monomers.[13]

The choice of solvent depends on the chemical nature of the template; polar solvents are suitable for polar templates, while non-polar solvents work better with non-polar templates.[21]

A research investigation concerning a Molecularly Imprinted Polymer [26] based on non-covalent interaction between methacrylic acid (MAA) and atrazine, shows the best performance with non-polar solvents such as toluene and dichloromethane. The study also demonstrates that MIPs based on covalent interactions exhibit reduced sensitivity to the solvent type employed. [26]

The solvent can be used also as porogen, playing a crucial role in controlling the polymer's morphology, controlling porosity creation and pore size. Different solvents can lead to polymers with more open or compact structures, depending on their

solvation ability. It is important to observe how the solvent affects the polymer network through swelling processes, as excessive swelling might reduce rebinding capability. For example, acrylate systems swell more in chlorinated solvents like chloroform and dichloromethane than in tetrahydrofuran or acetonitrile. [24]

The choice of solvent is essential to maintain specific interactions between the template and functional monomers during polymerization, regulating polymerization kinetics, and influencing the MIPs' rebinding capacity. Optimal rebinding performance is achieved when using the same or a very similar solvent to that used during imprinting; this suggests that it is necessary to maintain consistent solvation conditions. [24], [21]

1.1.5. Initiator of Polymerization

The polymerization initiator is a chemical substance that initiates the polymerization process, allowing the monomers to react with each other and with the cross-linker to form the cross-linked polymer. Initiators can be activated thermally, via UV radiation, or other methods.

The initiator generates free radicals, cations, or anions that start the polymerization reaction of the functional monomers and the cross-linker. This step transforms the mixture of reagents into a three-dimensional polymer network. [14]

The concentration and type of initiator used can influence the rate of the polymerization reaction, it's important to control this rate to obtain a homogeneous polymer structure.

The initiator can affect the microstructure of the resulting polymer, including the degree of cross-linking and the distribution of monomers within the matrix. These factors are crucial for the formation of recognition cavities specific to the template molecule.[14]

There are several types of initiators, for example [22]:

- Radical Initiators: These are the most common and include substances such as ammonium persulfate (APS) and benzoyl peroxide (BPO). They generate free

radicals that initiate the polymerization of vinyl monomers through thermal or photochemical decomposition.

- Cationic and Anionic Initiators: these compounds are less used; they start the polymerization by generating cations or anions. They are employed for specific monomers that polymerize better through ionic mechanisms.

The choice of initiator depends on the type of monomers used, the desired reaction conditions, and the final properties of the MIP. The compatibility of the initiator with the polymerization system is essential for an effective reaction. An efficient initiator ensures that the polymerization reaction proceeds quickly and completely, reducing the presence of unreacted monomers and improving the quality of the final polymer.[13], [19]

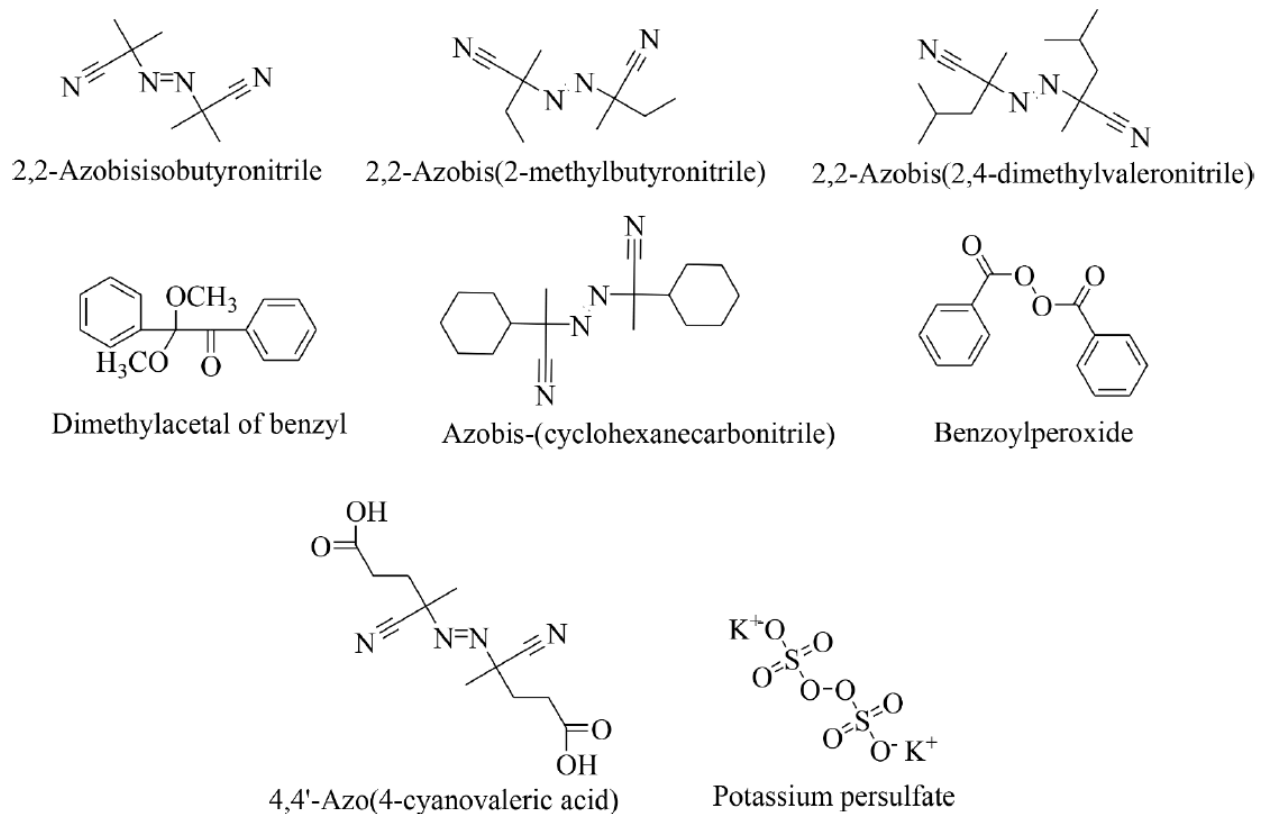


Fig. 5 The most used initiators in MIP's fabrication.[28]

1.2. Manufacture of MIPs: traditional and innovative methodologies

1.2.1. Strategies for the synthesis of Molecularly Imprinted Polymers

As previously mentioned, the synthesis of MIPs can be summarized into three main steps: formation of the pre-polymerization complex, polymerization, and template removal.

To analyse the state of the art of MIP synthesis in the literature, it is necessary to specify that the initial stage of interaction between the template and functional monomer, can be performed using different approaches. Specifically, three approaches are distinguished: non-covalent approach, covalent approach, and semi-covalent approach.

Non-covalent approach:

The non-covalent approach depends on non-covalent chemical interactions between the template molecule and the functional monomer, such as π - π interactions, hydrogen bonds, ionic interactions, and van der Waals forces.[29] After polymerization, the template is removed without requiring the disruption of covalent bonds, making this process straightforward. This approach offers a wide choice of monomers and templates and is preferred for its simplicity and economy. However, it can lead to a higher density of non-specific binding sites, necessitating optimization of reaction conditions to improve selectivity. It is useful when interactions between the template and functional monomer are sufficiently strong and specific to guarantee good MIP selectivity.[30]

Covalent approach:

This strategy involves the formation of a direct chemical bond between the template and the functional monomer, particularly a reversible covalent bond. During polymerization, this bond is maintained, and only after polymerization is it broken to remove the template. This approach aims to reduce non-specific binding. Some drawbacks include the complexity of template removal, which may require aggressive

conditions potentially damaging to the polymer. Additionally, the choice of monomers and templates is limited to those capable of forming reversible covalent bonds.[11] This method requires controlled reaction which may limit its versatility. It is useful when very high selectivity is required, provided that specific and controlled reaction conditions can be handled. [11]

Semi-covalent approach:

The semi-covalent approach combines aspects of the two previous methods: during polymerization, the template binds to the functional monomer through a covalent bond, while non-covalent interactions are exploited during rebinding. This approach allows for the creation of polymers with well-defined and specific recognition sites, offering greater stability compared to polymers obtained through non-covalent bonds. Moreover, template removal is generally simpler than in the pure covalent method. However, synthesizing MIPs with semi-covalent bonds is more complex and requires careful design to ensure that non-covalent interactions are strong enough for template recognition after its removal. It may be preferred when seeking a balance between the simplicity of non-covalent interactions and the selectivity of reversible covalent bonds.[11]

In conclusion, the choice of the approach depends on the selectivity and specificity of MIPs for the desired application, the manageable reaction conditions, and the complexity of the synthesis.

1.2.2. Methods of synthesizing MIPs

Free radical polymerization and bulk polymerization

Considering the available options and selecting an approach to produce MIPs, it is crucial to choose an appropriate synthesis method.

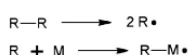
The synthesis methodologies discussed and analysed below can apply to all three primary approaches for binding the template molecule to the functional monomer in Molecularly Imprinted Polymers.

Many parameters must be evaluated during the synthesis of MIPs because they can influence the morphology, characteristics, and performance of the polymers. In particular: concentration of the target molecule, ration between binding agent, polymer and target molecules, washing and rebinding conditions, extent of the surface area. Although many authors [14], [20], [24], [23] have attempted to investigate and understand the role of various parameters in MIP preparation, achieving a comprehensive understanding of all of them remains challenging.

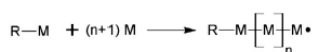
The synthesis of MIPs via free radical polymerization (FRP) is considered the most widespread methodology. [23] This reaction occurs under mild conditions (i.e., room temperature and atmospheric pressure) both in bulk and in solvent. The mechanism of free radical polymerization includes [11]:

- Initiation: Initiator (via heating or UV/visible irradiation) generates free radicals (R•), which attack the double bond of a monomer (M) forming an intermediate radical (R-M•).
- Propagation: The main phase of polymerization, where the chain grows through the addition of monomer molecules to the growing macroradical (R-M_n•).
- Termination: This phase can occur in different ways, for example through the recombination of two macroradicals or through disproportionation, leading to the formation of a C=C double bond and a C-H bond at the polymer chain ends.

Step 1. INITIATION

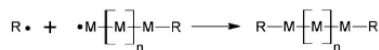


Step 2. PROPAGATION

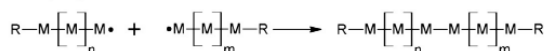


Step 3. TERMINATION

- coupling of initiator radical and macroradical



- coupling of two macroradicals



- termination by disproportionation



OTHER POSSIBLE REACTIONS

- transfer of free radical to another molecule (for example monomer)

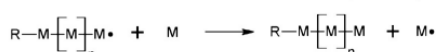


Fig. 6 General mechanism of FRP.[11]

Although FRP is widely used for the synthesis of MIPs, it does not allow for the control of the size, architecture, and number of growing macromolecules. Bulk polymerization is the most common form of free radical polymerization. This method is quick and simple: it is performed in solution, followed by lyophilization or drying. Then the materials are crushed and sieved.

As a result, irregularly shaped microparticles with a wide size distribution are often obtained [24]. However, the major limitation of this technique is that it produces samples with low selectivity and reproducibility because many binding sites are lost or damaged during the grinding process.

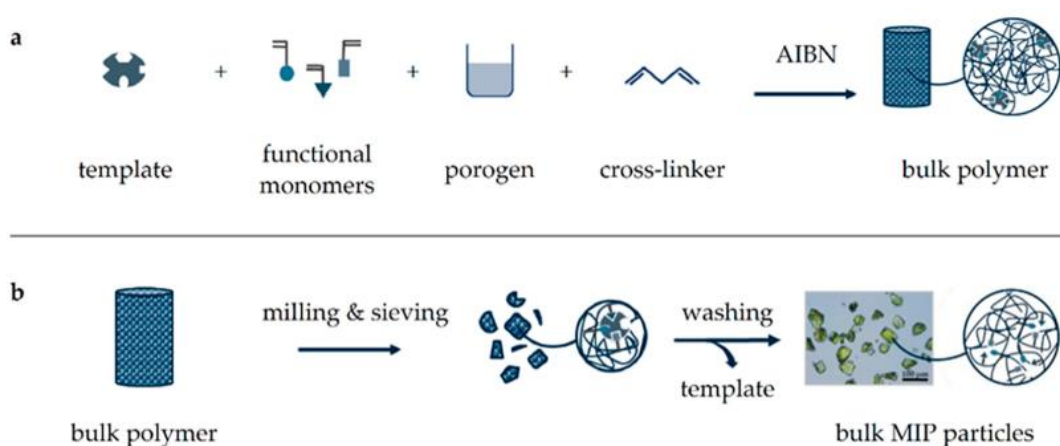


Fig. 7 Schematic illustration of MIP synthesis by bulk polymerization. First, a template, functional monomers, cross-linker, and radical starter (AIBN) are dissolved in porogen followed by heat-induced polymerization (a). The resulting polymer block is crushed milled, and sieved to obtain uniform particles, which are washed thoroughly to remove the template (b).[25]

To overcome the limitations of bulk polymerization, more advanced and complex polymerization methods have been developed to produce a wide range of MIPs. These methods include the production of particles, membranes, microspheres, molecularly imprinted monolayers, and in situ prepared monoliths. These advanced techniques address the difficulties and limitations associated with bulk polymerization. MIPs particles can be synthesized through precipitation polymerization, suspension polymerization, and emulsion polymerization.

Precipitation polymerization

Precipitation polymerization is a high-performance polymerization process that requires just one preparative step. This technique of polymerization produces homogeneous and spherical particles (usually less than $1\mu\text{m}$) but requires a big amount of porogen and template in the mixture. [5] Precipitation polymerization is a surfactant-free process where monomers are polymerized in dilute solutions without overlap or coalescence. Polymer chains do not polymerize together but instead, precipitate from of the solution. [5]

When compared to bulk polymerisation, this technique of polymerisation requires a high volume of solvent. Many factors affect the size of the produced particles, i.e., polarity of the solvent, reaction temperature, and speed of stirring, therefore the reaction conditions should be carefully monitored.[26]

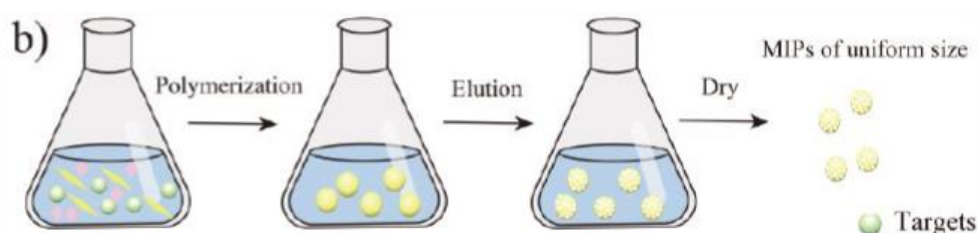


Fig. 8 Schematic illustration of MIP synthesis by precipitation polymerization.[27]

Suspension polymerization

Another commonly used method for the synthesis of MIPs is suspension polymerization. This technique allows to produce spherical particles, though they tend to be relatively large, ranging from micrometres to millimetres in size. Suspension polymerization typically occurs in water, but other continuous phases such as perfluorocarbon liquids and mineral oils can also be used. [11] The MIPs produced through this method, often exhibit poor recognition capabilities due to the influence of the medium. Despite this drawback, suspension polymerization is one of the few

methods that can be applied on a large scale, making it suitable for industrial applications.[11]

Emulsion polymerization

In the emulsion polymerization method, biphasic systems are prepared from a pre-polymerization mixture containing the initiator (polar phase), suspended in an oily solvent (non-polar phase) with a surfactant. The surfactant acts as a template for producing spherical micellar MIPs. This method enables the formation of monodisperse, spherical polymer particles and is particularly advantageous for creating MIPs with high surface areas and controlled porosity. The resultant MIPs can be used in various applications, including drug delivery, catalysis, and as selective filters in chemical sensors and chromatographic separations. [29]

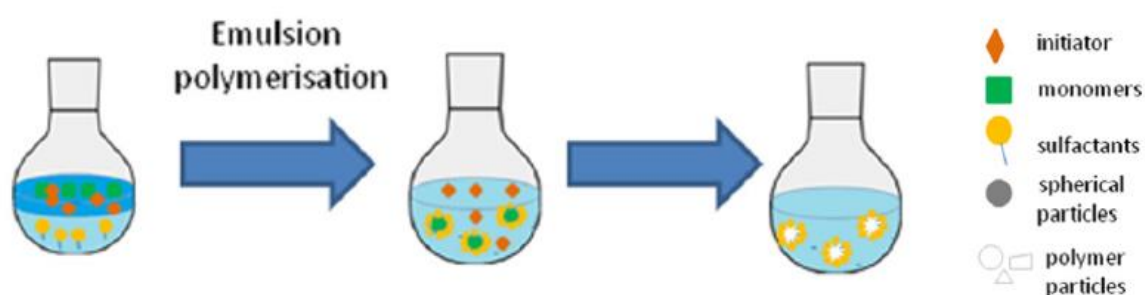


Fig. 9 Schematic Illustration of MIP synthesis by emulsion polymerization.[28]

The polymer particles typically range in size from tens to hundreds of nanometres. Water is commonly used as the continuous phase.

However, water's strong polarity and hydrogen bonding capacity, coupled with the presence of surfactants, can compromise the efficiency of the imprinting process.

These factors affect the stability of interactions between the template molecule and the functional monomers, which in turn can impact the imprinting process. As a result, emulsion polymerization is not widely utilized for the synthesis of molecularly imprinted polymers.

Surface imprinting polymerization

Surface imprinting polymerization, also known as surface lithography, involves grafting thin layers of MIPs on prepared beads to produce monodispersed products. Despite

its time-consuming nature, this approach yields surfaces suitable for separation or sensing applications in the form of thin imprinted layers.



Fig. 10 Schematic Illustration of MIP synthesis by surface imprinting.[27]

There are two main types of surface imprinting:

- **forming MIP films** on various substrates via spin-coating or deep-coating methods, in which a "stamp" produced from a self-assembled matrix of the template molecule is pushed into a partly polymerized film and kept in place until the film fully polymerizes. Binding sites are left on the MIP film surface after removing the stamp and template molecules. [15]
- **core-shell particles** that are produced using water-in-oil (W/O) emulsion polymerization, with the support material forming the core and a MIP surface (shell) coating it. The initial stage in this process is to synthesize the core material, which is typically silica particles and provides stability to the emerging core-shell MIP particles. The second phase involves emulsion polymerization to form a shell around the core particles. These approaches demonstrate the adaptability and specificity of surface imprinting in creating highly efficient MIPs for sophisticated applications.[29]

Multi-step swelling polymerization

Multi-step swelling polymerization offers several advantages, including the ability to create monodisperse particles and adjust porosity, thereby enhancing the specificity and efficiency of Molecularly Imprinted Polymers in separation processes. However, achieving these benefits necessitates meticulous control over reaction conditions and can be a complex undertaking. Despite these challenges, this technology has proven adaptable and effective across various fields, including chromatography, solid-phase

extraction, and chemical sensing, underscoring its broad applicability and success in polymer research. [11], [16]

The process begins with the preparation of seed particles, which absorb a water-soluble material to initiate their growth. Subsequently, a porogen and initiator dispersion are adsorbed onto these particles during a swelling process, facilitating pore development and polymerization.[5]

The addition of the template molecule, functional monomer, and cross-linker is a critical step in the process, facilitating complex formation through interactions. After polymerization, the template molecules are removed, leaving behind precise cavities that enable the selective recognition of target molecules.

1.3. Use of MIPs: debinding to rebinding procedure

Regarding the state of the art of washing and rebinding processes enabling the practical use of MIPs, these heavily depend on the type of selected template and the characteristics of the resulting polymer.[30]

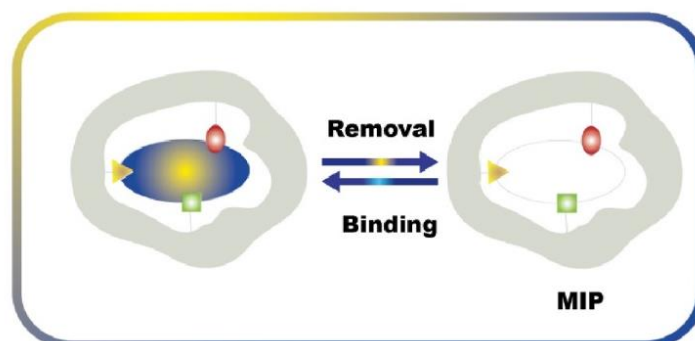


Fig. 11 Removal and binding.[30]

1.3.1. General overview of template removal

Washing (or debinding) is the process of removing the template molecule from the MIP after polymerization. This step, done with solvents, is essential to create specific cavities that allow the MIP to selectively recognize and rebind the target molecule. [31]

The total extraction of templates from MIPs is a challenging procedure due to the polymer network's characteristics and the imprinted cavities' attraction for the template.

Even after several washing cycles, it might be difficult to entirely remove the template. This happens mostly because the solvent cannot access the heavily cross-linked areas, or because the template is not soluble enough in the solvent to break contacts with the imprinted cavity. [31]

Furthermore, excessively aggressive washing conditions might cause deformation or rupture of the cavities, resulting in MIPs with limited selectivity. If MIPs still include template molecules, efficiency decreases because there are fewer slots available for rebinding.

Common solvents for template removal include mixtures of acids, bases, organic solvents, or aqueous solutions. Extraction can be performed through repeated washings, Soxhlet extraction, or other extraction techniques.[30]

Below, will be discussed some of the methods found in the literature[30].

Solvent extraction

The simplest and most widespread technique for template removal involves soaking MIP samples in a solvent. [31]This method uses organic solvents such as ethanol, methanol, acetone, or acetonitrile to solubilize and remove the template from the polymer. These solvents exhibit good template solubility to break the interaction with the binding cavity, as well as good polymer swelling properties to facilitate template release.[32]

The technique relies on washing cycles of the samples immersed in the chosen solvent under mild conditions. The washing cycles can be static, or the sample-containing solution can be incubated with gentle agitation (e.g., on a rocking platform) with or without heating.

During the procedure, the solvent is replaced multiple times, monitoring the amount of template released into the washing solution after each extraction cycle.[32]

The strength of this technique lies in its simplicity and straightforward experimental setup. However, it has several disadvantages, such as[32]:

- The long washing time, requiring hours or days.
- Aggressive solvents can damage the polymer.
- The method loses effectiveness when applied to templates that are difficult to solubilize.

- Significant waste of material.

Soxhlet extraction method

The Soxhlet extraction method is a laboratory technique used to extract compounds from solid materials using an organic solvent. This method, introduced by Franz von Soxhlet in 1879, is particularly useful for extracting lipids, pesticides, environmental contaminants, and other substances from solid matrices such as soils, plant tissues, or food.[31]

This is a cyclic extraction method that is repeated continuously for a predetermined period, usually many hours, allowing continuous and repeated extraction of compounds from the MIP particles.

The extraction process consists of filling a porous capsule into the extractor chamber with finely crushed MIP particles.

The solvent is placed into a flask attached to the lower end of the extractor chamber; then is heated, and the vapours rise through an ascending tube to the extraction chamber, where they condense and drip through the sample.

When the condensed vapor comes into touch with the MIP particles inside the cartridge, the template is removed; the solvent carrying the dissolved template descends through a siphon to the flask when a certain volume of liquid is achieved.
[31]

The key benefits of Soxhlet extraction are[33]:

- Using a hot solvent during extraction may improve template solubility.
- MIP particles are washed with fresh extracting solvent at regular intervals.
- The device is affordable, and the operator may be readily trained.
- It may be applied to almost any polymer matrix.

However, some disadvantages may also be highlighted[33].

- Long extraction times.
- Risk of temperature-induced deterioration of labile templates.
- High levels of organic solvent, which may raise ecological issues.

- Static nature of the process that reduces its efficiency.

Pressurized liquid extraction

The pressurized liquid extraction (PLE) technique, when water is used as the solvent, is called superheated water extraction or pressurized hot water extraction (PHWE).

During this procedure, polymer particles are placed in a stainless-steel container in a closed-flow system and filled with the selected solvent. Extraction takes place at high temperatures (up to 200 °C) and high pressures (500-3000 psi) for short periods (5-10 minutes). Then, the extract is expelled using a compressed gas (N₂), and the cycle can be repeated with new solvent.[32]

The use of high temperatures increases the solubilization capacity of the solvent, disrupting template-polymer interactions, and reducing the solvent viscosity for better penetration into the polymer. The application of high pressures offers additional advantages, such as the use of solvents at temperatures above the boiling point and access to inaccessible areas of the polymer.[31]

Although this method requires expensive instruments, extraction yields are excellent (>99%) with short times and low solvent volumes.

In addition, water as an extraction solvent is more environmentally friendly and economical than organic solvents, with PHWE applying high temperatures (~300°C) and pressures (10-60 bar). As temperature increases, water becomes more effective in solubilizing compounds of medium and low polarity, resulting in efficient template extraction.[32]

Microwave assisted extraction

The microwave (MW) energy is a type of nonionizing radiation with frequencies ranging from 300 MHz to 300 GHz and wavelengths ranging from 1 m to 1 cm, causing molecular motion via ion migration and dipole rotation without altering the molecular structure.[34] This extraction process uses MW energy to heat the extraction solvent in contact with the MIP and remove the template from the sample's polymer network.[32] Several factors influence the efficacy of microwave-assisted extraction (MAE),

including MW power and exposure duration, temperature, solvent volume, and solvent type, which all have a direct impact on template solubility and polymer solvation.

This process for template removal has several advantages, including quick extraction times (seconds to minutes), low solvent volumes that result in high extraction efficiencies, and the ability to automate.[31]

MAE can damage polymer cavities, thus using too high solvent temperatures on delicate MIPs should be avoided.[32]

Ultrasound assisted

Despite electromagnetic radiation, sound waves require a medium (solid, liquid, or gas) for propagation. Ultrasonic waves are mechanical vibrations that occur at frequencies greater than 20 kHz and involve rarefaction and compression cycles of materials. [34]Rarefaction reduces the density of molecules, whereas compression increases it. Wave compression and rarefaction in a liquid medium can produce acoustic cavitation, which causes bubbles to develop, expand, and finally burst. The bubbles cause shock wave damage and surface erosion on MIP samples, exposing new surfaces and resulting in enhanced mass transfer and template extraction. [32] Ultrasound-assisted extraction (UAE) has been effectively used to remove numerous templates, resulting in nearly total template removal utilizing both traditional organic solvents and their acid mixes. This approach may be used with an ultrasonic bath for extraction periods ranging from 10 to 60 minutes and solvent contents ranging from 30 to 200 mL. [32]UAE takes shorter extraction periods than the traditional Soxhlet approach and is less solvent-dependent.[31]

Supercritical phase extrusion

Supercritical phase extrusion uses substances that are above their critical temperature and pressure values. Supercritical fluids act as a solvent with low viscosity (comparable to that of gases) and high diffusivity, allowing effective template removal.

The most used supercritical solvent is carbon dioxide[32], because it has low toxicity, and it easily achieves supercritical conditions, plus it is effective for a wide range of templates and allows for complete and gentle removal.

The advantages of this method include reduced extraction time compared to other methods, lower use of organic solvents, and non-toxicity to the environment of the waste products of this process. However, the use of supercritical phase CO₂ as an extraction method is very limited as it requires specialized equipment and specific operating conditions, making the process very expensive and difficult to use.[32]

1.3.2. General overview of analyte binding

This paragraph aims to explore the current state of the art in the literature regarding the practical use of MIPs, specifically the rebinding process, in which the specific cavities present in the MIP selectively bind the target molecule, previously imprinted during the polymer synthesis. This process forms the basis of MIPs' recognition capability. In the case of non-covalent synthesis, the main steps of rebinding are[30]:

- **Target Exposure:** The MIP is exposed to a solution containing the target molecule. The target molecules migrate toward the specific recognition cavities within the polymer.
- **Specific Interactions:** Target molecules bind to the cavities through non-covalent interactions such as hydrogen bonds, dipole-dipole, and ionic interactions. The specificity of the binding arises from the complementarity of the cavity to the target molecule.
- **Binding Equilibrium:** The binding process reaches an equilibrium where a certain fraction of the target molecules is bound to the MIP cavities, while others remain in solution. This equilibrium depends on concentration conditions and solvent properties.

Batch Rebinding

Rebinding the analyte in solution is one of the most direct and simple method of exploiting the properties of MIPs.[31] In this approach, the MIP sample is dispersed in

a solution containing the target analyte. Due to specific interactions between the recognition sites of the MIP and the analyte, the last-mentioned is reabsorbed by the polymer.

The solution can be stirred, for example through magnetic stirrer [35], or allowed to rest under static conditions for a given period to allow maximum contact between the MIP and the analyte. Alternatively, a tilting platform can be used to set the solution in motion. This method is advantageous because of its simplicity and precise control of analyte concentration and incubation time. However, the solubility of both polymer and analyte may limit the effectiveness of rebinding. In addition, the presence of other components in solution may interfere with the binding process, reducing specificity.[31]

Electrochemical binding

This is a method used for rebinding ions on molecularly imprinted electrodes. This technique involves applying a potential difference to an electrode in solution, with or without the help of stretching the solution.[30] The most important parameter to be optimized is the choice of electrochemical potential. [36]The technique, used in some studies [36]such as Samandari et al. involves immersing the imprinted electrode in a solution containing ions, and after applying a potential opposite to the charge of the ion in solution for a specific period, under magnetic stirring conditions.

Gas Phase Rebinding

For the detection of volatile compounds, the rebinding of MIPs can occur in the gas phase. In this approach, the gaseous analyte, placed together with the MIP in a special chamber, is passed over or through the MIP, which absorbs the analyte thanks to its specific recognition sites. [37]This method is ideal for the rapid and sensitive detection of volatile compounds and can be used in portable devices for environmental monitoring or food safety. However, it requires controlled operating conditions and specific instrumentation to avoid interference from other gases or vapours present in the environment. It is not suitable for non-volatile analytes, limiting its application. The process includes several steps: polymer preparation, use of a sealed chamber for exposure to the gas mixture, introduction and exposure of the polymer to the gas

mixture, monitoring of interactions using analytical techniques and finally, removal and analysis of the polymer to evaluate the amount of target molecules captured and the polymer's selectivity. [37]

Each rebinding method has specific advantages and limitations; the choice of the most appropriate method depends on the application's requirements, the nature of the analyte, and the structure of the MIP. Often, combining different methods can offer optimal results by exploiting the strengths of each approach.

2. VAT 3D printing

2.1. Fundamentals of photopolymerization

Photoinitiated polymerization occurs when a light-sensitive system, called a photoinitiator, absorbs a suitable photon and reaches an excited state, leading to the formation of a reactive species capable of initiating the polymerization of monomers, that proceeds through chain reactions.[38]

Depending on the nature of the photogenerated reactive species and the chosen monomers, the polymerization can follow a radical, cationic, or anionic acid/base growing mechanism.

The radical mechanism consists of three phases: initiation, propagation, and termination. In the initiation phase, light activates the photoinitiator, generating a reactive species known as a radical. This radical interacts with monomers to form monomeric radicals. During the propagation phase, these monomeric radicals react with additional monomers, leading to a chain reaction. The termination phase occurs when the reaction ceases, typically through a combination process where two growing chains meet, and the radicals are inactivated.[39]

The ionic photopolymerisation mechanism is characterised using reactive species in the form of ions, often cations, to trigger and propagate the polymerisation reaction. Due to its slower speed and the need for additional treatments, cationic photopolymerisation is less common than radical photopolymerisation, especially in 3D printing technologies. Additional heat treatment after light-curing is often required to improve monomer conversion. However, ionic species may be less sensitive to the presence of oxygen than radicals, which can make the process more robust under different environmental conditions.[40]

Photocurable resins used in 3D printing primarily consist of photoreactive precursors and photoinitiators. Additional elements like additives, absorbers, and fillers can be included to enhance performance.[38]

- Precursors are monomers, oligomers, or prepolymers that solidify upon exposure to light, forming the resin's matrix and determining the final properties of the printed object. [38]
- Photoinitiators are crucial as they react with light to initiate the solidification process. Their type and amount significantly affect the kinetics and properties of the final print.[38]
- Additives such as dyes, inhibitors, and diluents are used to improve the resin's quality and control the printing process. [38]
- Absorbers help to manage light penetration to prevent over-polymerization.[38]
- Fillers like metal or ceramic powders can modify the printed material's physical and mechanical properties.[38]

2.2. Polymeric 3D printing: background and technologies

3D printing, also known as additive manufacturing (AM) or rapid prototyping, involves technologies that build three-dimensional objects using layer-by-layer deposition of materials.

It is important to highlight the difference between subtractive manufacturing and additive manufacturing. The first one consists of subtractive techniques, where the material of the initial solid block is progressively removed until the final object is achieved. In contrast, additive manufacturing builds the object layer by layer, adding material until the desired geometry is achieved. This approach significantly reduces material waste and contributes to environmental sustainability by reducing energy consumption compared to subtractive techniques. [41]

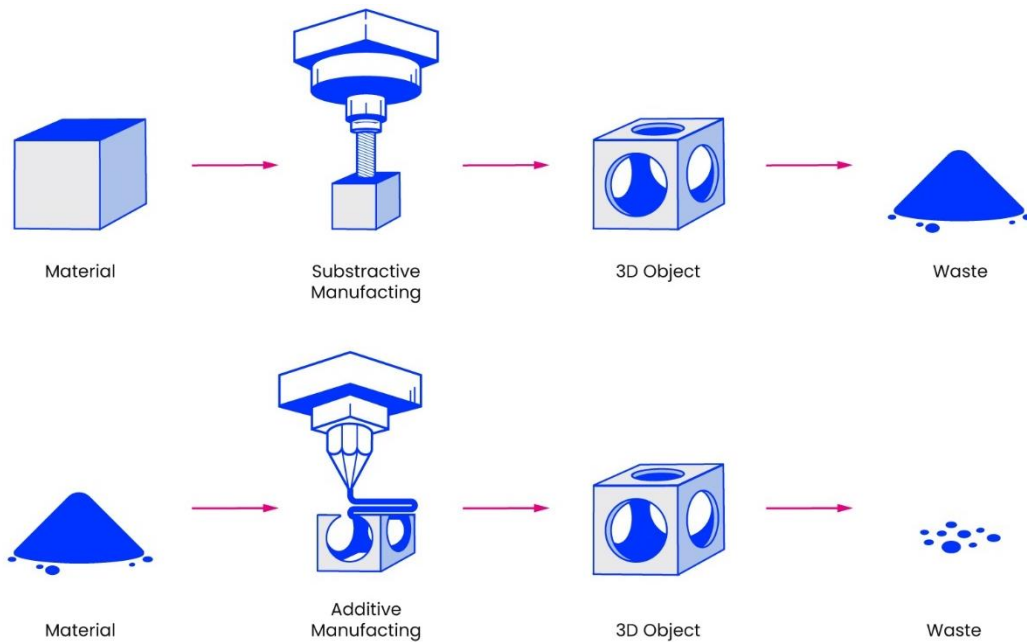


Fig. 12 Difference between CNC and 3D printing.[41]

In the last decades, AM is reshaping the product design, manufacturing, and distribution for end-users, significantly enhancing production efficiency and reducing costs. Moreover, it empowers consumers to exert greater influence over the manufacturing process by offering extensive input on the final product and facilitating customized production to meet individual needs.[42]

AM can effectively employ a diverse range of polymer materials in various forms and compositions, including composites, nanocomposites, continuous/discontinuous fiber-reinforced thermoplastic composites, and hybrid materials.[42]

AM offers significant advantages over traditional manufacturing techniques. [41] enables precise digital design reducing manufacturing inaccuracies and facilitates the creation of complex geometries that would be difficult or impossible to achieve with conventional methods. This capability supports rapid prototyping reducing the time required to bring products to market.

One sector in which the versatility of this technique is particularly useful, is the healthcare sector, where customised medical devices can significantly improve patient outcomes. Furthermore, the on-demand nature of AM supports agile supply chains, enabling faster and cheaper delivery of customised products and optimising resource deployment.

Despite these advantages, AM has limitations that restrict its full adoption in mass production. Challenges include dimensional limitations in large-scale object manufacturing, surface imperfections due to layer-by-layer printing processes, and the high initial costs associated with AM equipment and materials. Furthermore, AM adoption requires specialised skills and infrastructure, representing barriers to widespread implementation, especially for small and medium-sized companies that may lack the necessary resources and technological capabilities.[43], [44]

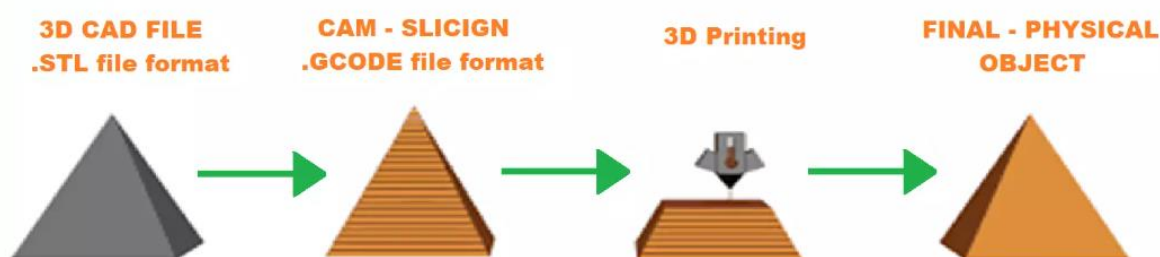


Fig. 13 Workflow of 3D Printing Process.[45]

In general, a 3D printing process follows a structured sequence of steps.[46]

Initially, a detailed 3D model of the object is crafted using sophisticated computer-aided design (CAD) software. Alternatively, the object can be scanned using advanced technologies like Magnetic Resonance Imaging (MRI), laser scanning, or Computer Tomography (CT).

Following the creation or scanning phase, the CAD model is converted into an STL (Stereo Lithography or Standard Triangulation Language) file format, which serves as the industry standard for AM machines. This conversion process involves translating the surface geometry of the CAD model into a precise mesh of triangles, where its number and size directly influence the printing resolution and fidelity.

Subsequently, the 3D model undergoes slicing into individual horizontal layers using specialized slicing software. Then the slicing software generates G-code instructions that include all the printing parameters such as layer thickness, printing speed, orientation, and temperature control.

When the G-code is loaded, the actual printing process starts. During this phase, the 3D printer progressively constructs the object. After this process, the final object undergoes post-processing procedures that typically includes treatments such as curing, sintering, and meticulous cleaning, aimed at refining the object's physical properties and surface finish to meet exacting specifications.

2.3. 3D printing methods

Printing methods can be classified into three main groups[47]:

- Extrusion-based techniques involve the transition of solid thermoplastic filaments to a liquid state as they pass through a heated nozzle. This melting allows precise deposition of the material, which rapidly cools and solidifies. Fused Filament Fabrication (FFF) and Direct Ink Writing (DIW) are commonly used methods within this category.
- Powder-based techniques, on the other hand, require the deposition of thin layers of powders that are subsequently pressed and compacted. These powders are then selectively melted using either a binder or laser radiation at desired locations. Selective Laser Sintering (SLS) exemplifies this approach, where powdered material is fused together in layers to create solid objects.
- In photopolymerization-based methods, a photosensitive resin composed of photopolymers and a photoinitiator undergoes a rapid solidification process when exposed to suitable light irradiation. This category includes stereolithography and vat photopolymerization techniques, like Digital Light Processing (DLP), which allow for quick and straightforward fabrication without the need for high temperatures.

2.4. VAT 3D printing

This method utilizes a vat of liquid photo-curable resins, from which solid products are fabricated by using a precise light source to selectively harden the photosensitive liquid into a three-dimensional solid in a layer-by-layer manner.

The light used for 3D printing can come from above, in the case of the free-surface approach (top-down printers), or from below, through a transparent vat, in the case of the constrained-surface approach (bottom-up printers).[42]

This technique is widely utilized in rapid manufacturing and rapid prototyping due to its ability to produce parts with exceptionally high resolution and excellent surface finish. It is particularly effective for creating concept models, rapid prototypes, and complex parts with intricate geometries. The Z-axis layer height define the resolution of a 3D printer, in a range between 25 microns and 300 microns on contemporary printers, allowing trade-off between speed and quality.

Irradiation can be performed by projecting the full pixelated picture onto the layer using Digital Light Processing (DLP) or by scanning each point of the desired portion with a laser in the Laser-SLA.[42]

2.4.1. Laser-SLA

Stereolithography (SLA) is the first developed AM process. In this method, a photosensitive polymer resin is exposed to a pinpoint ultraviolet laser, as illustrated in Fig.14. The printing platform, is situated in a tank filled with resin, ensuring that only a single layer of liquid resin covers it at any time. Upon contact with the ultraviolet light from above, the photosensitive resin solidifies in a layer. Subsequently, the layers are formed by exposing the resin according to the CAD data while the build platform is lowered. The platform moves along the Z-axis, while the laser moves along the X and Y axes.[48]

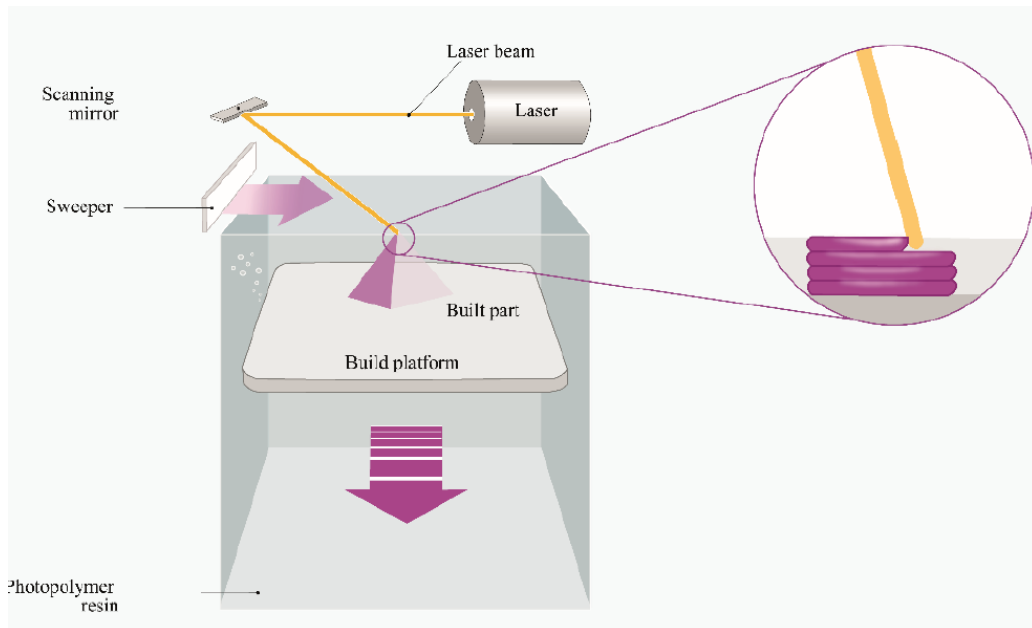


Fig. 14 Laser-SLA 3D printing configuration.[49]

2.4.2. Digital Light Processing (DLP)

Digital Light Processing (DLP) works in the same way of Stereolithography, with the difference that the light source is below the vat and the printing platform is above the resin bath. Furthermore, DLP uses a projector based on a digital micromirror device (DMD), enabling entire layers of the object to be printed in a single pass, significantly accelerating the printing process.[48]

Projection SLA employs resins of comparable viscosity and can be implemented using either free surface or constrained surface exposure, offering the same advantages and limitations as SLA.[50]

Standard DLP-based systems employ a light source with a typical wavelength of 365 or 405 nm and can achieve a resolution of 10 to 50 μm , contingent upon the magnification of the optics and the number of mirrors in the DMD system.[48]

The main benefit of this technique is that printing time is significantly decreased by lighting an entire layer at a time. Furthermore, less resin is used, because the sample doesn't have to be completely submerged in the vat, resulting in lower expenses.

The pixel-based exposure mechanism of this approach may result in imperfections on curved surfaces. Consequently, using the right optical technologies, the pixel size

must be decreased if high resolution is needed. The maximum size of the geometry is lowered due to picture shrinking caused by the DMD's fixed number of mirrors. For this reason, the large portions are frequently printed at a lower resolution than small portions.[48]

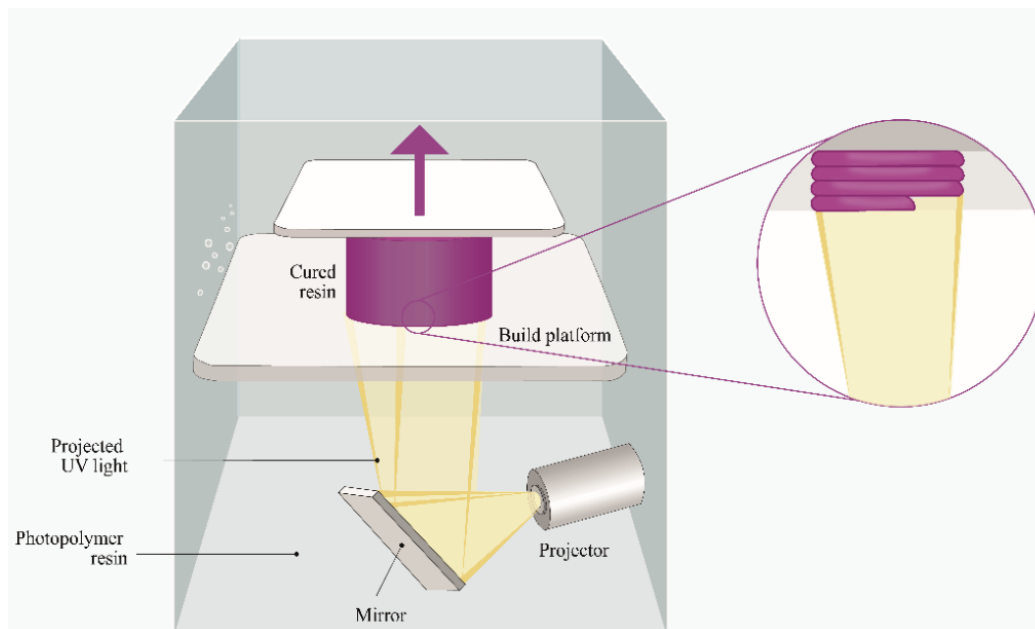


Fig. 15 DLP 3D printing configuration.[49]

2.5. 3D printing of MIP

3D printing of Molecularly Imprinted Polymers is an emerging field combining the advantages of MIP technology with the versatility of 3D printing.

The undefined architecture of MIPs, given by traditional synthesis techniques, is one of the main obstacles to their practical application.[51]

To overcome this problem, some studies aim to produce MIPs by 3D printing techniques to develop the best method for creating a precisely defined and self-standing three-dimensional object that retains all properties required for target recognition.[51]

An initial example involved the use of μ -SLA to fabricate 3D microstructures with adenine recognition sites[52]. Subsequently, two studies[53], [54] utilized two-photon photopolymerization technology (TPP-SLA). The first one [53] focused on replicating

high-resolution miniaturized 3D sensors, while the second one [54] aimed at creating 3D MIP structures with submicrometric resolution, incorporating one or more types of imprints. The maximum size achievable with the two-photon method is approximately 100 nm, making it unsuitable for large-scale MIP synthesis. In contrast, μ -SLA is employed to produce larger structures, even if one of its principal drawbacks is its limited printing speed.

In this moment, there is only one study [51] concerning the 3D structuring of MIPs using the DLP 3D printing technique, which successfully created highly structured, molecularly imprinted polymer (MIP) networks for copper (II) ion sequestration. Consequently, it is imperative to develop and evaluate a suitable 3D printing technique capable of rapidly and efficiently fabricating MIPs with complex architectures.

Given the promising results and the reasons, this thesis will investigate the fabrication and recognition capabilities of MIPs produced through DLP 3D printing.

3. Materials and Methods

The aim of this thesis is to combine Molecularly Imprinted Technology and VAT 3D printing to explore new perspectives in the synthesis and applications of highly specific and customized polymeric materials.

Below, the materials and methods used in this work will be reported, starting from the formulation to the various characterizations performed.

3.1 Ingredients of the Formulation

All the materials used in this thesis work, Oxytetracycline hydrochloride (OTC), methacrylic acid (MAA), Phenylbis(2,4,6-trimethylbenzoyl) phosphine oxide (BAPO), and dimethyl sulfoxide (DMSO) were purchased from Merck Company (Milan, Italy), except for Dipropylene Glycol Diacrylate (DPGDA) that was purchased by Allnex.

3.1.1. Molecule Template

The template used in this work is Oxytetracycline, a tetracycline class antibiotic.

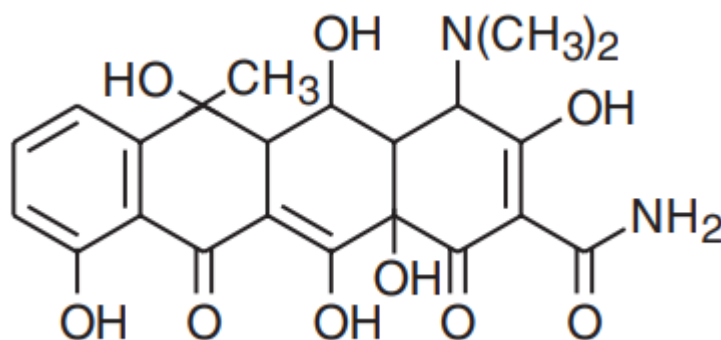


Fig. 17 Chemical structure of Oxytetracycline[23]

This molecule was chosen because tetracyclines are widely used in agricultural, human therapy, and veterinary medicine to treat a variety of bacterial diseases. Even if these drugs are therapeutically beneficials, their widespread and inappropriate usage has resulted in alarming environmental consequences. Indeed, after the administration more than 70% of the drug is expelled by the body through urine and feces in an active form, eventually polluting water drains.[55] Tetracyclines, particularly oxytetracycline, are very hydrophilic compounds and have little volatility,

which allows them to stay in watery environments. They can inhibit the biological activities of many different species in aquatic settings. The growth of antibiotic-resistant microbes is encouraged by these residues, raising the danger of infection. As the introduction chapter noted, there is a significant risk to both human and animal health from this occurrence, which is known as antimicrobial resistance. Antibiotic residues have also been found in cow's milk[65] and other food items animal derivatives, which exacerbates the issue of antibiotic resistance and may have negative health impacts on consumers, including endocrine abnormalities and allergic responses.

3.1.2. Functional Monomer

The functional monomer employed in the formulation is methacrylic acid. This choice is due to its high affinity with the template molecule and the presence of the carboxyl group, which can form hydrogen bonds with the target molecule.

In the literature, most MIPs created through non-covalent imprinting are based on methacrylic monomers, such as methacrylic acid.[56]

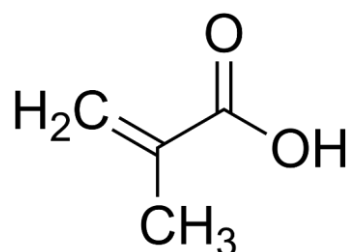


Fig. 16 Chemical structure of Methacrylic Acid[57]

3.1.3. Crosslinker

The crosslinker used in this work is Dipropylene Glycol Diacrylate (DPGDA). This compound is a bifunctional crosslinker, it has two reactive acrylate groups and it's compatible with a wide spectrum of functional monomers used in MIP formulations.

Its chemical structure gives the final polymer some flexibility, but, at the same time, the crosslinking supplied by DPGDA is stiff enough to prevent the imprinted cavities from collapsing, ensuring the MIP's functioning.

DPGDA's low viscosity makes it easier to mix and handle pre-polymer solutions and helps avoiding problems during 3D printing or casting operations by limiting the production of flaws or air bubbles inside the polymer.[58]

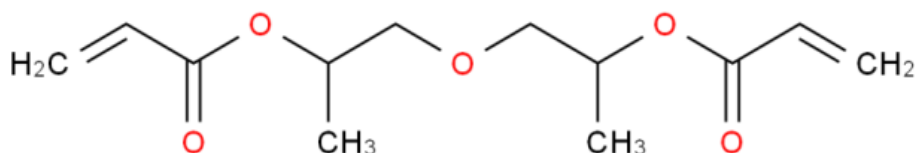


Fig. 17 Chemical structure of Dipropylene Glycol Diacrylate (DPGDA)[58]

3.1.4. Solvent

The solvent in this MIP's formulation is dimethyl sulfoxide (DMSO).

DMSO is a polar aprotic solvent, it has a high dielectric constant, making it capable of dissolving many monomers, crosslinkers, and templates used in MIP formulations. [59] This characteristic allows a homogeneous pre-polymer solution, which is necessary to create a uniform polymer network.[59]

Another important DMSO's feature is the high boiling point, allowing the polymerization process to take place at high temperatures without evaporating. [59]

From a practical aspect, DMSO is miscible with water and many organic solvents, allowing the template molecules to be easily removed from the polymer matrix, leaving well-defined imprinted voids. Lastly, DMSO is less toxic and safer to handle than other solvents that may be employed in MIP formulations.[59]

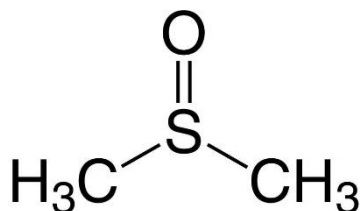


Fig. 18 Chemical structure of Dimethyl Sulfoxide (DMSO)[60]

3.1.5. Photoinitiator

The photoinitiator chosen is phenylbis (2,4,6-trimethylbenzoyl) phosphine oxide (BAPO).

It absorbs the emission wavelength (385 nm) of the utilized 3D printer, producing free radicals, which start the polymerization of monomers and crosslinkers in the resin formula.[61]

Other important characteristics of this compound are thermal stability, solubility, compatibility with resin components, safety profile, and suitability for rapid and controlled polymerization, all of which are required for successful 3D printing processes. [61]

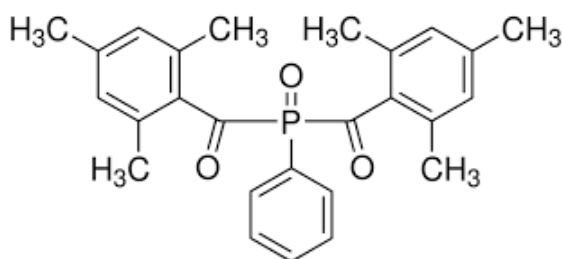


Fig. 19 Chemical structure of phenylbis (2,4,6-trimethylbenzoyl) phosphine oxide (BAPO)[62]

3.2. Preparation of the Formulation

3.2.1. MIP resin: Molecularly Imprinted Polymer

Regarding the synthesis strategy of MIPs (various options were mentioned in paragraph 1.2.1), this thesis employs the non-covalent approach as the binding strategy between the template and the functional monomer. Below there are the relative quantities of the compounds within the photopolymerizable resins obtained and the creation process.

The MIP formulation was prepared with the following weight ratios between template (OTC), functional monomer (MAA) and crosslinker (DPGDA):

$$\text{MIP} \rightarrow \text{OTC:MAA:DPGDA} = 1:5:20$$

Then 1 phr (per hundred resins) of BAPO and 15 phr of DMSO were added.

The preparation of the MIP formulation consists of three main steps:

- The first step is the polymeric precursors preparation, consisting of DPGDA mixed with BAPO, then put in sonication for at least ten minutes until the photo initiator is completely solubilized.
- The second step is the preparation of the pre-polymerization complex by combining OTC, MAA and DMSO. These components are mixed by magnetic stirring, for at least one hour, to allow the proper self-assembly between template and functional monomer.
- The last step consists of mixing the two components previously prepared, adding dropwise the polymeric precursors to the pre-polymerization complex, always under magnetic stirring at a speed of about 700 rpm, increasing them if a creation of a suspended phase is noticed.

In case at the end of the procedure the resin is not perfectly transparent and homogeneous, it is sonicated for 10 additional minutes. At the end of this procedure most of the formulations results clear, indicating effective dispersion of all the ingredients.

3.2.2. NIP resin: Non-Imprinted Polymer

This second formulation is used to obtain “control” samples to investigate the difference between specific and aspecific adsorption. To make this comparison the NIP resin has all the components of the MIP resin, excluding the template, so that the cavities characteristic of molecularly imprinted polymers will not be created.

The ingredients are the functional monomer, crosslinker, photo initiator and solvent, with the same weight percentages as the MIP resin.

The preparation of the NIP formulation consists of two main steps:

- “Polymeric precursors” preparation as for MIP resin.
- Addition of MAA and DMSO to those- IN this second case, it is not necessary to carry out perform dropwise addition under magnetic stirring, since it is not necessary to reach complete solubilization of the OTC and creation of the pre-polymerization complex.

3.3. DLP 3D Printing

3.3.1. DLP 3D Printer

In this work, the samples are produced through 3D printing photopolymerization. The printer used to make the samples is the ASIGA MAX UV-X27 printer, made by the company ASIGA.

This printer employs DLP (Digital Light Processing) technology, which allows for high resolution and accurate detail in prints. Equipped with a 385 nm LED UV digital light source. The printer has a resolution of 27 μm on the x-y plane and 1–500 μm along the z plane. The building platform is 51.8 x 29.2 mm^2 and capable of printing objects up to 75 mm tall. The platform heads vertically from bottom to top, and the sample is printed backwards. The printer is controlled by its software, ASIGA Composer, which allow control of all the printing parameters.



Fig. 20 ASIGA MAX UV-X27 DLP 3D printer[63]

3.3.2. Printing Process, Cleaning and Post-Curing

The samples were printed with two different geometries:

- “dot”, bulky disks 500 μm thick
- “gyroids” 1.5 mm high

The printing process was carried out by placing approximately 1 mL of resin inside the printer tank and performing careful optimization of the printing parameters divided into different ranges.

The most carefully investigated printing parameters, divided into different ranges, are the thickness of the printing layers, the light intensity, and the exposure time of every printing layer.

The first printing range is called “burn in”, that is the printing range that allows the sample to properly adhere to the printing platform. After that, there may be one or several ranges depending on the geometries chosen and the resins used.

Once these printing parameters were optimized, several samples were made, and different steps were performed after printing the samples and removing them from the printing platform.

- *Cleaning*: Once printed, the samples were immersed in a solvent such as ethanol or isopropanol and sonicated for 1-2 minutes. This step aims at removing the excess of resins on the parts.
- *Post Curing*: after the washing step, the samples were dried with lab paper and then exposed to UV light, to complete the polymerization reaction and improve material properties, such as strength, hardness and dimensional stability. After this step, the samples are ready for testing. The samples are post-cured for 3 minutes each side by Asiga® Flash Cure Box (light intensity 10 mW/cm²).[64]

3.4. Debinding, rebinding, washing after rebinding process

3.4.1. Debinding o washing: washing conditions

To perform the template washing step, the samples were put in a flask and immersed into the washing solution. The flask is then placed on top of a tilting platform so that the fluid is set in motion to achieve a more effective washing.

After several hours, the washing liquid is refreshed, and the Ultrasound-Assisted extraction method is carried out by placing the flask inside an ultrasonic bath.

This process is repeated until the template is completely removed.

The composition of the washing solution is acetic acid (AA) and Methanol (MeOH), with ratio AA:MeOH=1:9.

To compare the rebinding process on samples that were subjected to the same conditions, the washing step was performed both for MIP samples and for NIP control samples, even though the latter do not contain the template molecule.

3.4.2. Rebinding process: features of the rebinding experiment

Once samples were fabricated, those were incubated in a solution that contains the template used for the imprinting process, to evaluate the ability of binding sites to capture the target molecules. The quantity of template still present in solution after the binding to the polymer is measured and compared to the initial quantity value provided, resulting in an adimensional and percentage parameter that describes the sample's removal capacity.

$$\% \text{ Removal} = \frac{(C_i - C_f)}{C_i} \times 100$$

Where:

- **C_i** is the concentration (μM) of the starting rebinding solution
- **C_f** is the concentration (μM) measured in each time step of the rebinding experiment

In this study, the rebinding solution is composed of OTC dissolved in demineralized water, prepared at known concentrations. Both MIPs and NIPs samples were tested.

The sample is typically placed in a multiwell plate with 750 μL of rebinding solution for each well. The plate was then placed on the rocking platform and in the incubator, to maintain a constant temperature throughout the experiment.

After different time steps, 250 μL of the rebinding solution have been collected every 1, 3, 5, 24 hours and placed in another multiwell plate; then a preliminary analysis of this solution was carried out using the UV-Visible plate reader, to visually check whether the samples under analysis have captured the template.

The absorption spectrum of the rebinding solution collected was compared to the spectrum of the starting solution, at a wavelength value of 355 nm that is the characteristic absorption peak of the template molecule. The optimal result to achieve is a decreasing in the peak over the time, compared to the starting value. The final step is to determine the concentration values using a calibration curve and to calculate the parameter previously described as the removal percentage.

3.4.3. Washing after rebinding process

At the end of the rebinding process, to test the ability to reuse samples, they were washed again.

The washing conditions are the same as those used in the first washing step with the same washing solution.

This attempt to reuse filters is carried out with a perspective to significantly reduce the costs associated with their production and use, to increase their efficiency and reduce the waste produced. This reuse would make MIPs more versatile, allowing them to be used for a variety of applications.

3.5. Characterization Methods

In this paragraph, the various methodologies used to characterize the liquid resins and the printed samples will be presented and analysed.

3.5.1. Rheology

The rheometer is a measuring device used to investigate the rheological properties of a material, including viscosity, storage modulus (G'), loss modulus (G''). There are two main ways of operating with this device: oscillatory rotation and continuous rotation. The rheometer measures the material's reaction to shear stress while it is in continuous rotation mode, which requires applying a stable rotating force to the material sample. The flow curve, which shows the connection between shear stress and the material's shear rate, is the primary result of this test. Several rheological properties, including viscosity, may be determined from the flow curve. Viscosity can change depending on temperature, duration, or shear stress.[65] In this thesis study, the viscosity (η) of the unpolymerized resin (both for MIP and NIP resins) was determined as a function of the shear rate ($\dot{\gamma}$) using the shear rate test. The instrument used was Anton Paar MCR 302, and the configuration chosen was the parallel plate.



Fig. 21 Anton Paar MCR 302 Rheometer.

3.5.2. Photo Rheology

The study of photo rheology analyses how a material's rheological characteristics change due to light irradiation, especially to visible or UV light. This may include

modifications to the material's characteristics, polymerization kinetics or any other photoinduced process.[65]

The oscillatory time sweep test was used to determine the formulation's polymerization kinetics and see how it is affected by the presence of the template molecule, comparing MIP resin to NIP resin.

In this oscillatory time sweep test the values of G' and G'' are tracked over time in this test while the oscillation frequency and deformation amplitude are maintained constant.

The Amplitude Sweep is a prerequisite test that must be completed before performing the Oscillatory time Sweep test. The moduli's linearity range must accommodate the oscillation amplitude selected for the oscillatory time sweep. [65]

During the Amplitude Sweep, the formulation is tested at a constant frequency while the oscillation amplitude increases, and the moduli of the material are assessed. The linearity range (LVE) is the range of oscillation amplitudes within which G' and G'' remains constant. The amplitude of deformation is chosen to guarantee that it always falls within the LVE region.

When the material is in a liquid-viscous phase, such as monomeric formulations, usually the viscous modulus is greater than the elastic modulus w . On the other hand, the elastic modulus is greater than the viscous modulus when the material is solid. Consequently, during cross-linking, the test curve should show an increase in both moduli's values as well as an inversion point, defined as gel point, where the elastic modulus becomes greater than the viscous modulus. Since the gel point marks the transition from liquid to solid, it is very significant for 3D printing processes, since having indication of the time required can help in the definition of printing parameters.[65]

Both the slope of the growth segment of the two moduli and the delay time (the interval of time between the lamp's activation and the gel point) are significant factors for assessing polymerization kinetics. The slope is more closely associated with the reaction's propagation rate, whereas the delay time is more closely tied to the polymerization reaction's beginning phase.[65] One crucial aspect of the setup for this

photo rheology test is the need for a quartz or glass plate to allow light irradiation (supplied from below).

All rheological tests were carried out at 25°C, and the selected gap between the two plates was 200 µm.

The test was conducted using the same plate-plate arrangement rheometer as described in paragraph 3.5.1. A broad-spectrum Hamamatsu LC8 UV lamp was employed as light source.

The test consists of three main phases:

- Beginning of the measure, monitoring the values of G' and G'' .
- The light is turned on, after 60 seconds and the sample is irradiated for a certain amount of time.
- Continuous monitoring of G' and G'' until the plateau value is reached.



Fig. 22 Hamamatsu LC8 UV lamp

3.5.3. UV/visible spectroscopy

UV-Visible is an analytical method that measures the absorption or emission of light in the ultraviolet (UV) and visible (Vis) sections of the electromagnetic spectrum. This approach is widely used to determine the quantity of radiation absorbed or emitted by an analyte. UV-Visible spectroscopy is based on matter's energy that is quantized, and radiation photons, that can be absorbed or emitted by matter if the energy associated with the photon matches the energy difference of the species' permitted transitions.

This analytical approach allows the collection of spectra resulting from the interaction between electromagnetic radiations and the matter. In the literature, there are different spectroscopic approaches that differ depending on the species researched, the radiation-matter interaction detected, and the area of the electromagnetic spectrum investigated.[66]

In this thesis this technique was employed to evaluate the filtering capacity of the samples through an indirect measurement of the absorbance of the rebinding solution in which the samples were dipped.

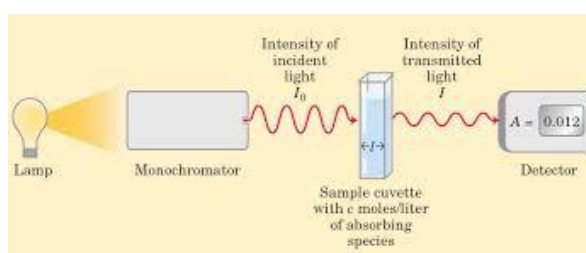


Fig. 23 Schematic representation of UV-visible absorption spectroscopy[67]

The Bouguer-Lambert-Beer law serves as the mathematical framework for measuring light absorption in gases and solutions in the UV, visible, and infrared ranges.[68]

$$A = \log(I_0 \cdot I) = \varepsilon \cdot l \cdot c$$

From which derives:

$$\varepsilon = \frac{A}{c \cdot l}$$

Where:

- A is the absorbance.
- I_0 is the intensity of the monochromatic incident light (so before passing through the sample).
- I is the intensity of the monochromatic transmitted light (so after passing through the sample).
- ε is the molar extinction coefficient of the substance that causes the absorption of radiation.

- c is the concentration of the light-absorbing substance.
- l is the optical path length of the sample.

The Lambert-Beer law, which is fundamental for spectrophotometric analysis, can only be applied in certain conditions. Firstly, the incident radiation must be monochromatic, the analysed solution must be transparent and homogeneous; light can be scattered by suspended particles or precipitates and provide incorrect results. The law is applicable at relatively low concentrations; deviations caused by molecular interactions are common at high concentrations. Absorbance must also be directly proportional to the path length of the cell and the concentration of the absorbing species. Another crucial condition is that the substance must not emit light (fluorescence or phosphorescence) when excited by the incident radiation. Lastly, to allow precise measurements of light intensity, the detector used must have a linear response to the intensity of the incident radiation.

With these conditions, the Lambert-Beer law can be successfully used to calculate the concentration of an absorbing species in solution.

Specifically, the BioTek™ Synergy™ HTX Multi-Mode Microplate Reader (Fig.26) was used, performing absorbance tests between 250 nm and 500 nm with intervals of 1 nm.[69]



Fig. 24 BioTek™ Synergy™ HTX Multi-Mode Microplate Reader[69]

3.5.4. Calibration Curve

In the context of absorbance analyses, it is necessary to determine a calibration curve at known concentrations plays to discuss properly the results, enabling precise quantification of unknown sample concentrations.

Consequently, defining a calibration curve is also essential for correcting potential instrumental and systematic variations. By using the same instrument and experimental conditions for both the standard solutions and unknown samples, these errors are minimized. [66], [68]

The calibration curve is obtained by measuring the absorbance of a series of standard solutions of the substance of interest dissolved in a solvent with known concentrations, keeping all experimental conditions constant. It's also important that the instrument is calibrated to zero absorption by creating a "base line" using a cuvette filled only with the solvent. By plotting a graph of absorbance versus concentration, a single wavelength is selected (usually the location of the absorbance peak), and the absorbance at that wavelength is plotted against the concentrations of the solutions, then applying a linear regression method, an equation describing this relationship is obtained.

This equation, usually in the form:

$$y = m \cdot x + b$$

Where:

- y represents absorbance
- m is the slope (or extinction coefficient)
- x is the concentration
- b is the intercept.

Another important value is the R^2 value, if it is close to 1, it indicates that a good fit was achieved.[70]

When the calibration curve is complete, it can be used to calculate the sample's

unknown concentration. In this work the solvent used is water, in which OTC is solved, whose characteristic absorbance peak is 355 nm.

3.5.5. FTIR Spectroscopy in Attenuated Total Reflectance (FT-IR ATR)

Attenuated Total Reflectance Fourier Transform Infrared Spectroscopy (ATR-FTIR) is an advanced analytical technique used to characterize the chemical composition of materials by analysing their infrared absorption properties.[71] This method is renowned for its capacity to examine samples that are solid, liquid, or paste without requiring complicated preparations; as a result, it is very adaptable and helpful in a variety of domains, including biological sciences, chemistry, and materials science.

The core idea behind ATR-FTIR spectroscopy is to measure the amount of infrared light absorbed by the sample when it meets an ATR crystal with a high refractive index. These crystals are usually composed of germanium or diamond.

The ATR crystal is exposed to infrared light, which experiences several complete internal reflections there. A little amount of radiation reaches the sample's surface at a micrometre

depth on each reflection, enabling interaction with the functional groups.[72]

The vibrational frequencies of the chemical bonds in the sample are matched by the selective absorption of specific infrared wavelengths caused by this interaction.

The instrument's output is an FTIR spectrum, which shows absorbance (or transmittance) as a function of the wavelength (or wavenumber) of the infrared light.

The spectrum shows the molecular vibrations corresponding to each peak, giving a chemical "fingerprint" of the material. [72]

ATR-FTIR is the ideal technique for quick and non-destructive material analysis.

In this thesis work, this characterization was performed on both the antibiotic powder in its solid state and the two liquid formulations, MIP and NIP, in their liquid state. Additionally, some samples were analysed immediately after printing and after the washing process, specifically after the removal of the template, to obtain detailed information about the chemical composition and structural changes of the materials at various stages of the study.

For the solid-state analysis, the antibiotic powder was directly placed in contact with the ATR crystal to obtain its characteristic infrared spectrum. This initial characterization served as a reference for the subsequent analyses of the formulations. The liquid formulations, MIP and NIP, were analysed in their liquid state to assess the presence and distribution of the functional groups in their respective compositions. This step was crucial to understand the baseline chemical structure of the polymers before any further processing. [72]

After the 3D printing process, the printed samples were subjected to ATR-FTIR analysis. This provided insights into how the printing process might have affected the chemical integrity and composition of the materials. It also allowed for the comparison of the printed samples with their pre-printed liquid formulations to detect any potential changes or interactions that occurred during printing.

Furthermore, performed at the end of the washing process, this analysis can be employed to confirm the successful removal of the template. In fact, comparing the spectra collected before and after washing it is possible to verify the efficiency of the template removal process, by observing the absence of the signal related to OTC.

In this thesis, the Thermo Fisher Scientific Nicolet™ iS50 Spectrometer was utilized in attenuated total reflectance (ATR) mode, covering the range from 4000 to 550 cm^{-1} . 32 scans were collected with a resolution of 2 cm^{-1} .

3.5.6. Atomic Force Microscope (AFM)

An excellent instrument for studying the physical characteristics and surface morphology of materials at the nanoscale is the Atomic Force Microscope (AFM). The AFM sticks out because of its capacity to investigate surfaces with sub-nanometric resolution, therefore capturing molecular and atomic features.[73] The investigation utilizes the force interactions that occur between the sample surface and a minuscule tiny tip that is fixed on a sensitive cantilever. With this method, surface topography may be captured by applying different forces, and to retain the best resolution, force feedback continuously modifies the distance between the tip and the sample. The cantilever tip oscillates all over the sample surface during scanning. A laser detector that captures shifts in the cantilever position is used to track the tip movement. By precisely recording surface topographical differences, this force feedback keeps the

tip and surface at a consistent distance. Furthermore, this analytical instrument permits the examination of surfaces under liquid, vacuum, or air conditions, allowing for the detection of structural alterations or surface-liquid interactions in a variety of settings.[74] The data collected during the scanning are processed to create high-resolution images of the sample surface.

In this thesis work, this analysis is conducted to study the surface of 3D printed MIPs. The instrument used is the Bruker Innova operated in tapping mode, with a resonance frequency set at 300 kHz. The probe tip used is the RTESPA-300. The images were post-processed using the Gwyddion software.

3.5.7.3D Scanner

A 3D scanner was used to compare the printed geometry to the one made with CAD software to assess the printing quality of some of the sample, of the samples printed with 'Gyroid' CAD geometry.

The instrument used to perform this characterization is the 3Shape E4 scanner made by the Danish company 3Shape, located in Copenhagen, Denmark.

Some of the features of this scanner are the presence of four 5 MP cameras and the high scanning accuracy that reaches values of 4 μm (ISO 12836).[75]

After performing a careful calibration of the instrument, to reduce light reflection, the sample is gently coated with magnesium stearate before being placed on the scanning platform, then, the scanner creates a digital model of the item that was tested. The last step of this analysis is to compare the digital model created by the scanner to the CAD model using Convince software from 3Shape. The output of the software is a colorimetric map that reports differences between the two files, with a legend.



Fig. 27 3Shape E4 scanner

4. Samples printing and results analysis

As discussed earlier, this investigation aimed to fabricate Molecularly Imprinted Polymers using DLP 3D printing, an innovative approach necessitating further research and analysis. This thesis presents the initial steps and aims to lay the groundwork for future developments in this field.

All the experiments performed in this thesis work follow the same workflow. The steps involved are:

- Preparation of the formulation.
- Selection of CAD geometry.
- Optimization of the printing parameters and printing process.
- Post curing of samples.
- Removal of the template molecule.
- Rebinding process.
- Data analysis.

4.1. Formulation's preparation and characterization

4.1.1. Formulation's preparation

The formulation is obtained following the steps described in the previous chapter. The MIP resin results in a yellow-coloured liquid resin as can be seen in Figure 28, for the presence of OTC.



Fig. 25 MIP formulation.

4.1.2. Formulation's characterization

RHEOLOGY

As described in the previous chapter, rheological tests were conducted to analyse the viscosity of the MIP and NIP formulations. The results obtained from these tests are presented in the following figure (*Fig.29*). Evaluating the graph, it is evident that, at low shear rates, the viscosity of the NIP formulation, represented by the orange curve, is significantly higher than MIP's one, represented by the blue curve. As the shear rate increases, both resins exhibit shear-thinning behaviour, characterized by a decrease in viscosity with increasing shear rate. The MIP formulation demonstrates a more stable viscosity profile across the tested shear rates. At higher shear rates, both resins converge to similar low viscosity values, suggesting that both materials exhibit comparable behaviour under these conditions. In brief, measured viscosity values are compatible with the DLP printing process.

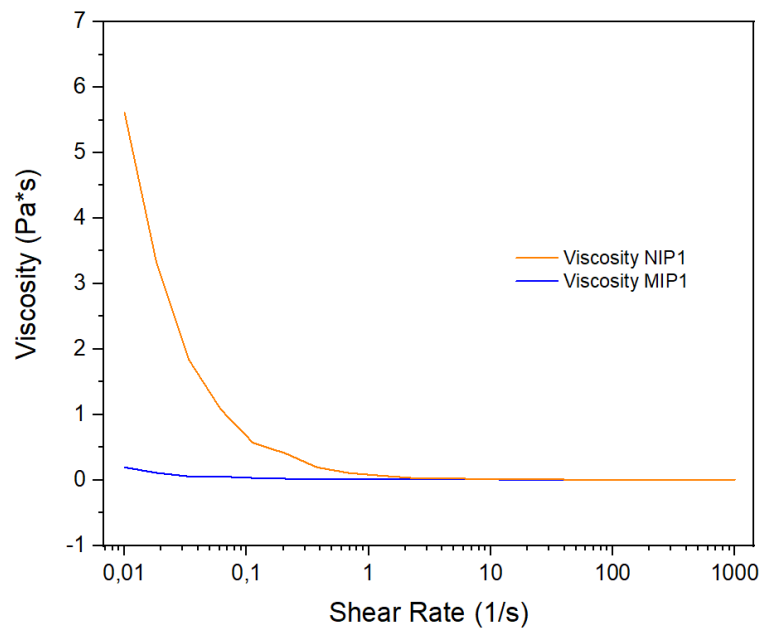


Fig. 26 Viscosity of MIP and NIP formulations under continuous shear rate sweep.

PHOTO RHEOLOGY

After investigating the viscosity of the solutions, a photorheological test was conducted to analyse the behaviour of the storage modulus (G') over time.

As expected, initially, both the MIP and NIP formulations exhibit very low G' values, as for liquid formulation. At the 60-s mark, the UV light source is switched on and the G' behaviour was followed. The graph in the figure (Fig. 30) shows a steep rise in the G' modulus, indicating the beginning of polymerization and the resins' transition from the liquid to the solid state.

The differences in the rise times and the magnitude of increase between MIP and NIP can be attributed to their distinct molecular architectures and compositions. As expected, the NIP, green curve, demonstrates a sharp and rapid increase in storage modulus, reaching its maximum value relatively quickly, approximately in 20 seconds, suggesting a fast and efficient photopolymerization process. Conversely, the MIP, blue curve, delayed rise of G' and reaches a slightly lower maximum value compared to the NIP. This behaviour can be related to the presence of OTC molecule, which might play a two-fold effect in the cross-linking process. On the one hand, the delayed polymerization can be associated by the absorption of the antibiotic in the light's irradiation range (385 nm), which competes with the PhI in photon absorption,

decreasing photopolymerization efficiency. On the other hand, the presence of OTC can be a steric hindrance for double bonds reaction, decreasing final modulus and eventually overall cross-linking density. These differences in MIP and NIP's polymerization kinetics will lead to distinct values in certain printing parameters, which will be discussed later.

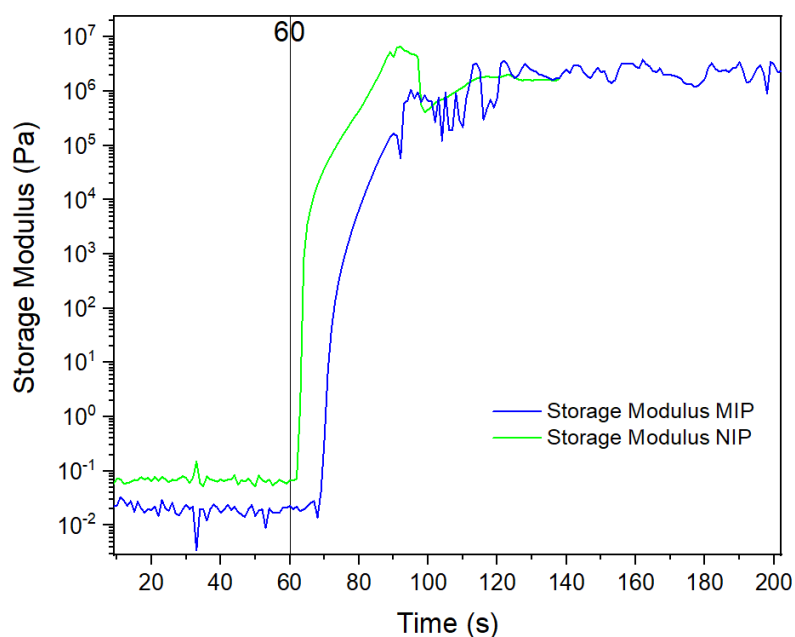


Fig. 27 Real-time photorheological measure of the MIP and NIP formulations

4.2. 3D printing process optimization and characterization

4.2.1. CAD geometry

The Rhinoceros software was used to create the CAD models of the samples to be printed. All the geometries created share a common diameter of 9 mm. This diameter was chosen for practical reasons, ensuring that the dots and gyroids fit precisely inside the 48-multiwell plate used in the experiment.

DOT

The first geometry employed is a simple dot with a diameter of 9 mm and a height of 500 μ m. This geometry was used to make both MIP and NIP samples.

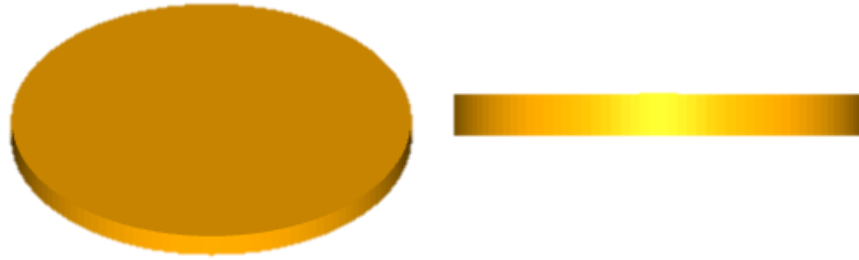


Fig. 28 Dot geometry, with 9 mm diameter and 500 μm height.

GYROIDS

The second geometry used is a three-dimensional structure with a complex, undulating geometry. It presents a circular base and consists of a series of curved shapes that intertwine to form a network with circular openings. The structure has cavities and empty spaces within it, and it has a periodic symmetry.

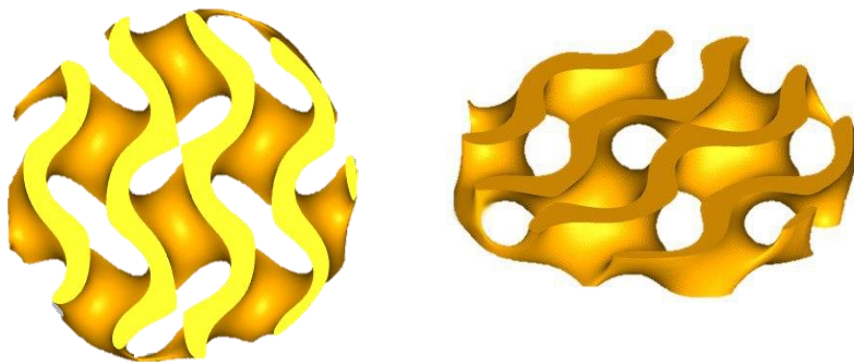


Fig. 29 Gyroid geometry, with 9 mm diameter and 1.5 mm height

4.2.2. Printing process and parameter optimisation

The printing parameters listed below were obtained following careful optimization. This process involved varying one parameter at a time until identifying the best combination to ensure proper sample printing. The first goal pursued was to obtain samples adhesion to the printing platform, and not to the resin vat. To this aim, the parameters investigated were basically light intensity, exposure time, and layer thickness.

Once the parameters for achieving a correct print were obtained, further optimization was carried out to produce prints that increasingly match the original CAD design in

terms of resolution. Optimizing the printing parameters for simple geometries, such as dots, is also necessary to ensure that the samples are sufficiently rigid without being overly fragile, which would indicate overexposure to UV light.

Two ranges have been created to print dots with MIP and NIP formulation: burn-in and range 1. The printing parameters are summarized in Table 1 and Table 2. Picture of the printed samples are shown (Fig. 33-34).

The presence of the antibiotic, as seen in the photo rheology results, slows the reaction kinetics but enhances the printability of the resin due to its characteristic absorption peak around 385 nm. The antibiotic acts as a dye, increasing the z-axis resolution.[76]

Tables 1 and 2 illustrate the variations in exposure time to the light source and the intensity of the light beam.

MIP DOTS


DOT MIP	Burn-in	Range 1
	0-200 (µm)	200-500 (µm)
Light Intensity (mW/cm ²)	50	47
Exposure Time (s)	32	35
Slice Thickness (µm)	25	50

Table 1 Optimized printing parameters for MIP dots.

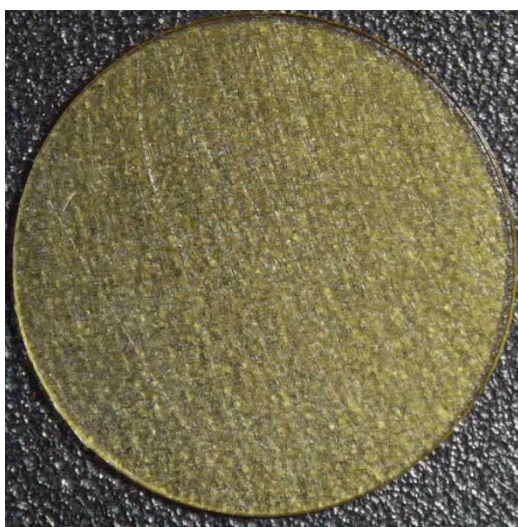


Fig. 30 Top view of a MIP dot. Image obtained with an optical microscope.

NIP DOTS


DOT NIP	Burn-in	Range 1
	0-200 (μm)	200-500 (μm)
Light Intensity (mW/cm^2)	20	20
Exposure Time (s)	3.5	4.5
Slice Thickness (μm)	25	50

Table 2 Optimized printing parameters for NIP dots.



Fig. 31 Top view of a NIP dot. Image obtained with an optical microscope.

MIP GYROIDS

Two ranges have been used to print gyroids with MIP formulation: burn-in and range 1. The printing parameters are summarized in Table 3.

After successfully printing several samples with the dot geometry, subsequent prints were made using the second geometry, the gyroids. These were exclusively printed with the MIP resin as a proof of concept to demonstrate the quality and suitability of the resin for printing.

The values in the table 3 indicate a slight variation in the printing parameters from the ones used for the dot geometry with MIP resin. This variation is attributed to changes in the geometry, which necessitated further optimization of the parameters.

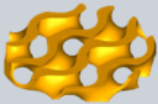
GYROID MIP	Burn-in	Range 1
	0-200 (μm)	200-1500 (μm)
Light Intensity (mW/cm^2)	50	47
Exposure Time (s)	32	35
Slice Thickness (μm)	25	40

Table 3 Optimized printing parameters for MIP gyroids.



Fig. 32 Top view of a printed MIP gyroid. Image obtained with an optical microscope.

4.2.3. Printed samples' characterization

3D SCANNER

The 3D scanner is the first characterization performed on the printed samples. This scanning process is conducted to analyse the print fidelity. As shown in the colour map, the printed gyroids exhibit good print fidelity, with differences between the CAD model and the printed product of at maximum $\pm 50 \mu\text{m}$ in nearly all areas of the sample. The larger deviations, indicated by the blue and red colours, are due to the unique geometry of the sample and the scanner's difficulty in accurately measuring all the cavities present in the sample.

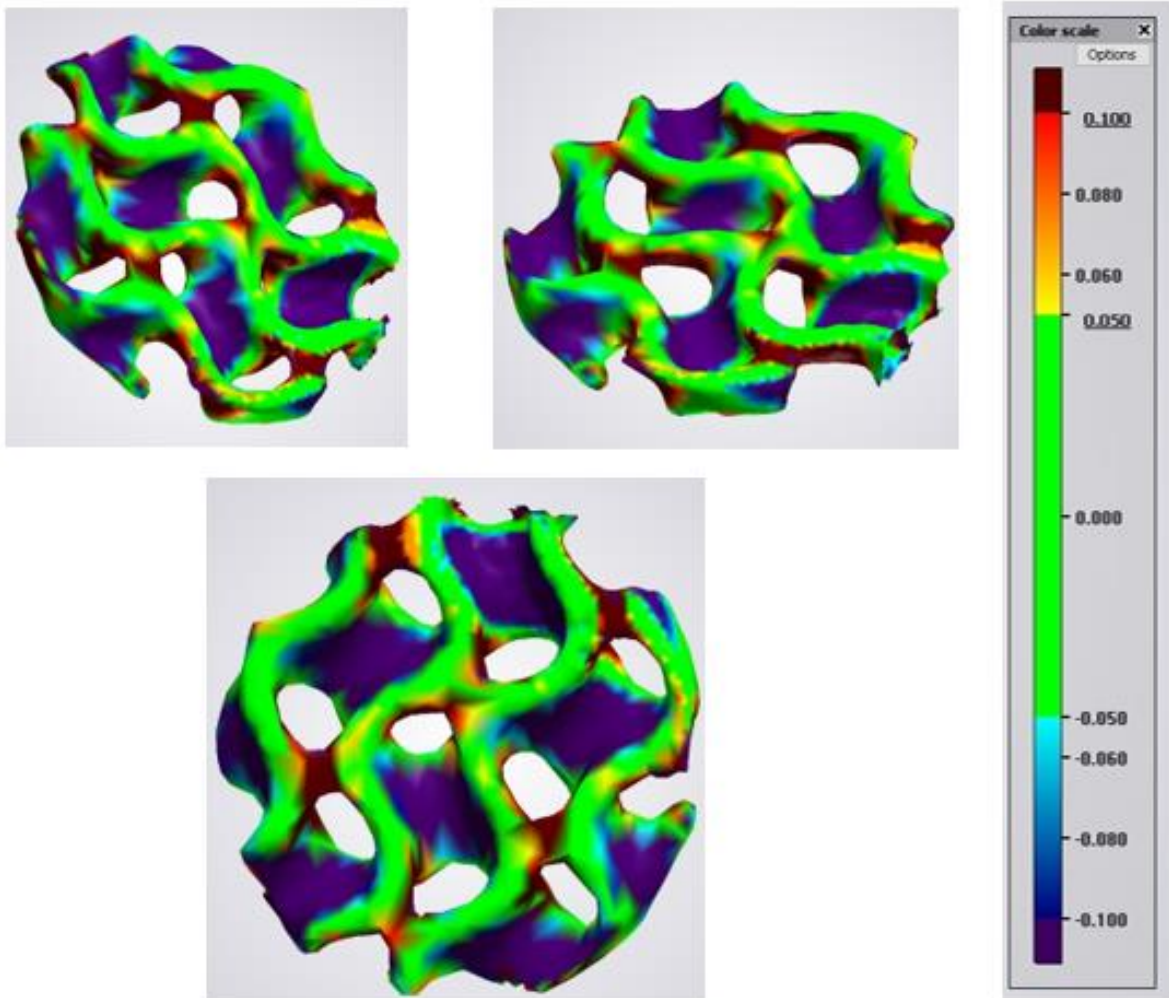


Fig. 33 3D scanning of gyroid with MIP Formulation.

ATOMIC FORCE MICROSCOPE

The objective of this AFM analysis was to investigate the surface morphology and roughness of the polymer samples. For this purpose, the MIP and NIP samples were printed directly onto a transparent slide, which is necessary for placement in the AFM sample chamber.

The results were processed using Gwyddion software, which facilitated the generation of the topographical map presented in Figure 37. This 3D map provides detailed information on the surface roughness of the 3D-printed samples, allowing a comparison between MIP and NIP.

Approaching this experiment, two investigation goals were pursued:

1. Being able to observe the surface of the samples. In this sense, this test was challenging because AFM is usually performed on ad-hoc prepared flat surfaces, while in this case the test was performed on unknown 3D printed surfaces.
2. Eventually, to observe differences between MIP and NIP surfaces.

In case of success of this experiment, further experiments can be envisaged, observing the surfaces after every MIP step of the process here studied.

Fortunately, both samples were measurable, and surface maps were obtained. Interestingly, specific different characteristics of the surfaces were not evidenced. Notably, the surface roughness was found to be very low, with values in the range of tens of nanometers, indicating that both MIP and NIP samples possess very flat and regular surfaces.

Further measurements will subsequently be necessary to detect the presence of the template. For instance, one could conduct this measurement on a MIP sample, followed by subjecting it to the template extraction process, and then repeating the measurement to evaluate the presence of significant differences.

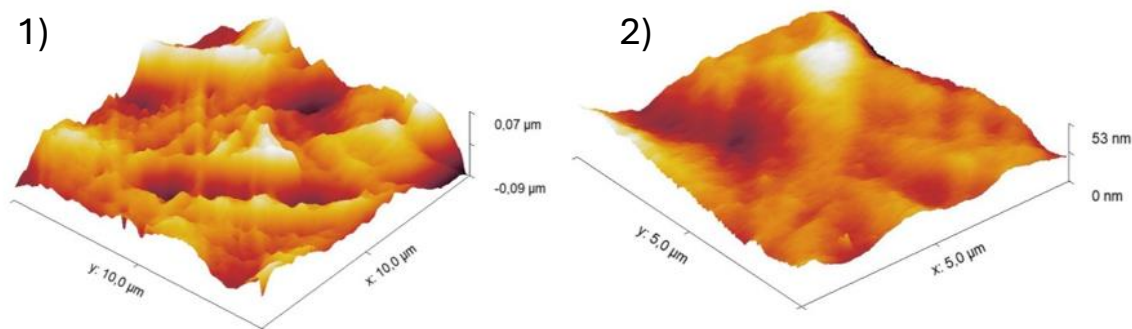


Fig. 34 Topographic surface map of 3D-printed MIP (1) and NIP (2) samples.

4.3. Debinding

After the printing process, each sample undergoes post-processing, which includes removal from the building platform, cleaning in ethanol via an ultrasonic bath to eliminate unpolymerized resin, and post-curing in a UV chamber for enhanced structural durability. Once these steps are completed, the samples are ready for template extraction.

The washing method used is the one described in the previous chapter, the figure 38 presents the gyroid sample before (1) and after (2) the template debinding procedure.

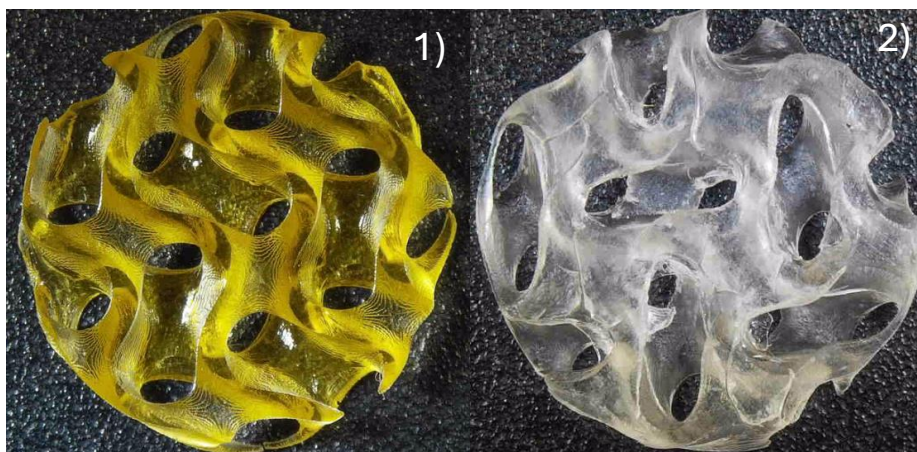


Fig. 35 Gyroid sample printed with MIP resin, before washing (1) and after washing (2).

Moreover, it is important to specify that the washing solution needs to be changed when it becomes saturated with antibiotics, in our case, OTC. This is necessary because there is a risk that the OTC will be reabsorbed by the sample instead of being eliminated. Furthermore, if the absorption spectrum obtained by the plate reader is

saturated, it becomes impossible to determine whether additional OTC was released in subsequent washings. Additionally, this washing procedure is time-consuming and requires the constant presence of an operator to analyse the washing solutions at regular intervals.

The graph below shows the results of a test conducted on the effect of the temperature of the ultrasound bath during the ultrasound-assisted debinding procedure.

The spectra are obtained by measuring the washing solution on dot samples.

The graph shows the results compared to the control solution Methanol and Acetic Acid (9:1).

The conditions of the three different tests are:

- First Test (1 hour): The absorbance is measured after one hour of ultrasonic (US) treatment, with one sample at a temperature of 50°C and the other at room temperature (Tamb).
- Second Test (2 hours): Following the first hour of treatment, the washing solution is replaced with a fresh solution, and the absorbance is measured after two additional hours of US treatment, with one sample at a temperature of 60°C and the other at ambient temperature.
- Third Test (4 hours): the washing solution is replaced with a fresh solution, and the absorbance is measured after two more hours of US treatment, with one sample at a temperature of 60°C and the other at ambient temperature.

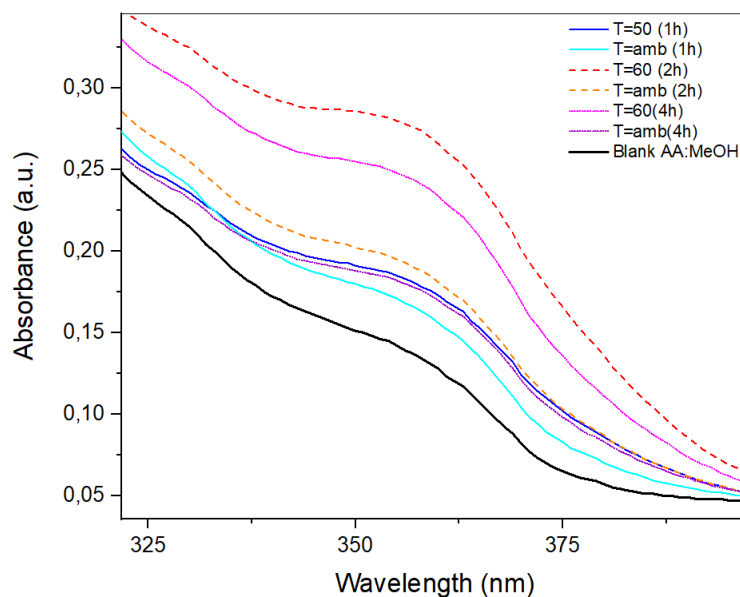


Fig. 36 Effect of the temperature of the ultrasound bath during the ultrasound-assisted debinding procedure.

Based on the results, it can be concluded that the temperature of the ultrasonic bath is a crucial variable in the ultrasound-assisted washing method. Indeed, increasing the bath temperature enables greater extraction of the template within the same time frame, thereby expediting the process.

FTIR SPECTROSCOPY IN ATTENUATED TOTAL REFLECTANCE

Infrared (IR)-ATR spectroscopy was performed both on the two liquid resins, Oxytetracycline powder and on the printed samples. The samples after the debinding procedure are also compared.

In the figure below, the absorbance spectra are presented. It's possible to notice that a significant peak in the spectrum of the powdered antibiotic, at 1580 cm^{-1} , is also present both in the spectrum of the MIP formulation and in the spectrum of the printed MIP sample. This peak can be related to aromatic groups of OTC. In contrast, this peak is absent in the spectra of the NIP formulation and the printed NIP sample, indicating the absence of the OTC molecule. Finally, we can compare the MIP and NIP samples after the template extraction process. It is noted that the spectra are overlapping, and

both do not show the peak at 1580 cm⁻¹, indicating the correct removal of the antibiotic.

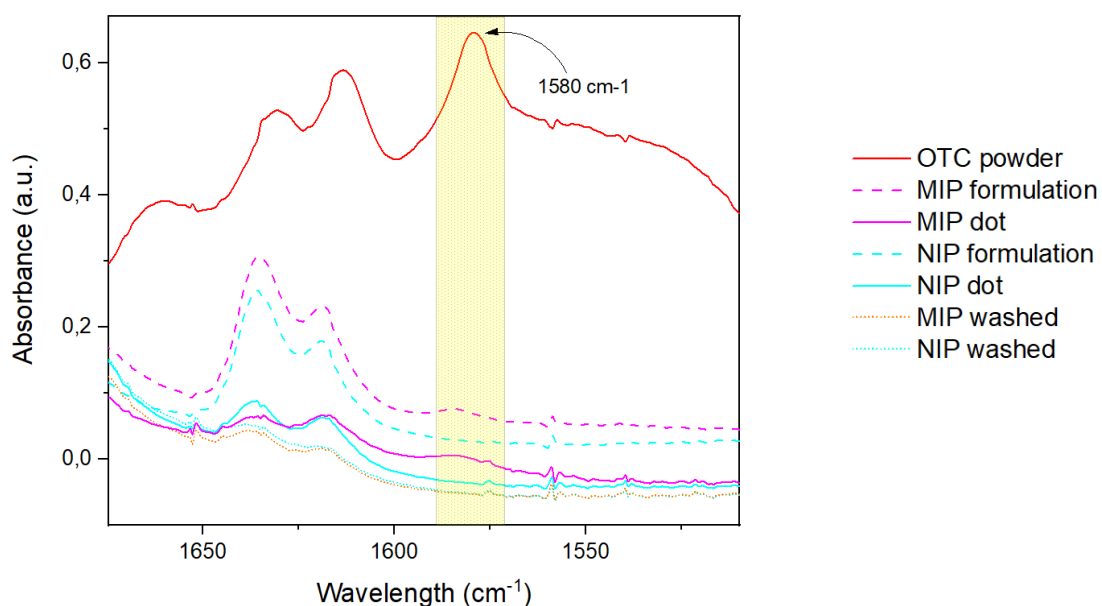


Fig. 37 ATR FT-IR spectra of both liquid formulations and printed samples, and the pure antibiotic in powder.

Another important information that can be derived from this measurement is the acrylate conversion (*Table 4*). This parameter identifies how many monomers participated in the polymerization reaction by calculating how many C=C bonds characteristic of acrylates open up to form C-C bonds and contribute to the polymer chain. This data is obtained following the decrease of the peak corresponding to the double bonds (1630 cm⁻¹), specifically by calculating the area under the peak. Once calculated, this area is normalized against the area of a peak unrelated to polymerization (such as the peak at 1730 cm⁻¹ corresponding to C=O bonds). With these two parameters, the degree of polymerization can be calculated using the formula:

$$\text{Degree of crosslinking \% (G\%)} = \left(1 - \frac{A_{1630}(\text{crosslinked})/A_{1730}(\text{crosslinked})}{A_{1630}(\text{formulation})/A_{1730}(\text{formulation})}\right) \times 100$$

		Formulation	Printed Sample	G%
MIP	A ₁₇₃₀	10,95	17,3	89,8%
	A ₁₆₃₀	1,0461	0,169	
NIP	A ₁₇₃₀	11,15	19,66	80,8%
	A ₁₆₃₀	0,9596	0,3245	

Table 4 G% calculated for MIP and NIP samples.

In both cases double bond conversion is very high (> 80%), in good agreement with photorheology experiments. However, MIP conversion appears slightly higher than NIP one. In this context it must be noted that final conversion can be influenced by several factors, and in particular chain mobility of the growing macromolecules. Usually, this test is cross-checked with evaluation of the insoluble fraction (gel content). However, in this case this experiment cannot be performed due to the presence of OTC in MIP, which is released in the washing step, and consequently would affect the results. In any case, it is possible to state that both the specimens result highly cured and suitable for following tests.

4.4. Rebinding experiments

4.4.1. OTC calibration curve

To create the calibration curve for OTC, different molarities of the solution has been prepared: 150, 125, 100, 75, 50, 40 and 30 μ M. The starting point was the preparation of the stock solution, starting from dissolving 18 mg of OTC into 15 mL of demineralized water. Then, from the stock solution, all the other solutions were then obtained, by dilution.

Each one was subjected to absorbance spectrum analysis using the plate reader and the absorbance spectrum with H₂O as the blank has also been recorded.

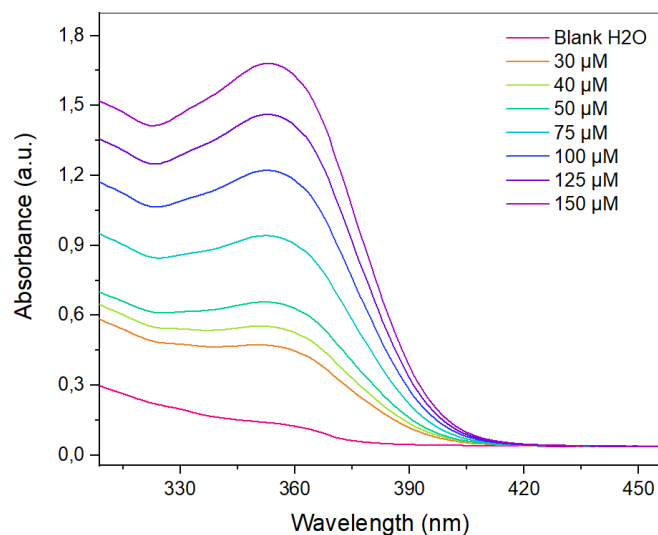


Fig. 38 Absorbance spectra of rebinding solutions with OTC in water.

The values of concentration from 0 μM (blank solution) to 150 μM, have been associated with their respective absorption values at wavelength of 355 nm. This results in the graph in the figure 42.

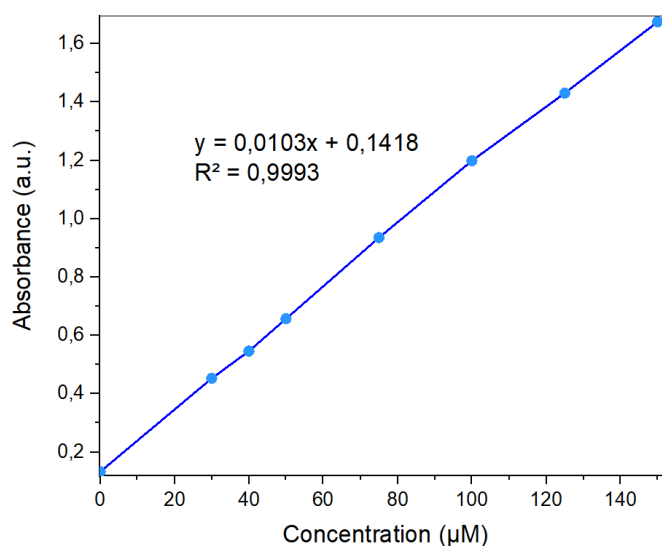


Fig. 39 Calibration curve.

The linear graph (Fig.42) obtained by correlating absorbance data with known concentrations is the calibration curve, whose equation is:

$$y = 0,0103x + 0,1418$$

The dispersion of data points around the fitted regression line is quantified using the coefficient of determination, R^2 . This value ranges from 0 to 1, with larger R^2 values generally indicating a better fit of the regression model to the observed data.[70] In this case the R^2 value is 0.9993, indicating an excellent fit.

Once the curve and its equation are obtained, it will be possible to associate a concentration value with each absorbance measurement taken with the instrument.

4.4.2. Stability test of the rebinding solution

Before conducting the rebinding experiments, a stability test was performed on the rebinding solution alone. The test compared two different conditions:

1. The rebinding solution was placed in the wells of a multiwell plate, which was then positioned on a *tilting platform* and kept at uncontrolled room temperature on the laboratory bench top.
2. The rebinding solution was placed in the wells of a multiwell plate, which was then placed inside an *incubator* set to maintain constant environmental conditions at 26°C.

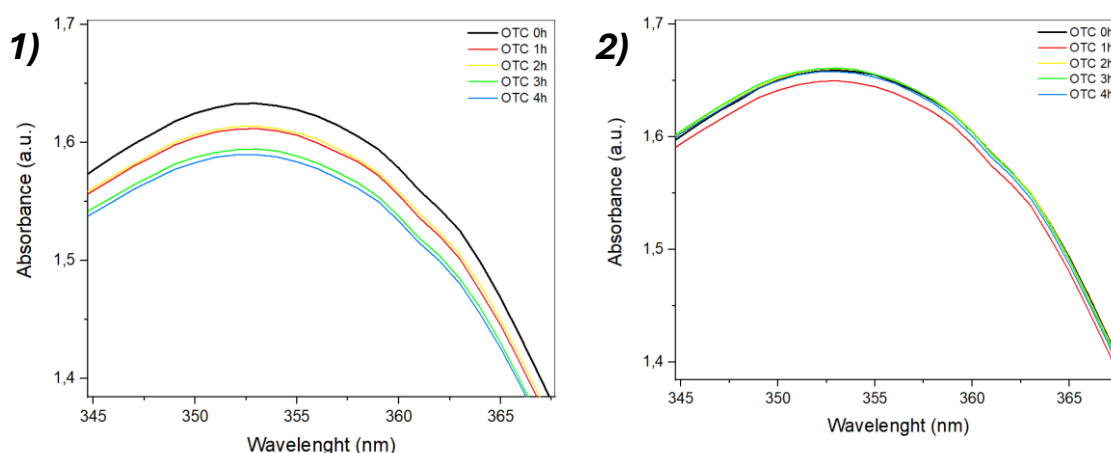


Fig. 40 Absorbance spectra of rebinding solution at different time step in first condition (1), and second condition (2).

The results indicate that, under controlled and constant conditions (Condition 2), the solution exhibits more stable behavior over time compared to the other condition

investigated. This suggests that the antibiotic dissolved in water is quite susceptible to environmental changes. These findings established the conditions for subsequent experiments, which were all conducted in an incubator with controlled temperature.

4.4.3. First experiment, DOT1: MIP and NIP

The initial rebinding experiment was conducted on triplicate samples of MIPs and NIPs. The template-deprived samples were incubated in a 100 μM solution following the procedure described in the previous chapter. The absorbance spectra obtained at various time points, specifically, 1, 3, and 5 hours of immersion, are presented in *figure 44*. In the presented graph, the spectra of the MIP samples, depicted with a solid line, are compared with the NIPs, shown with a dashed line.

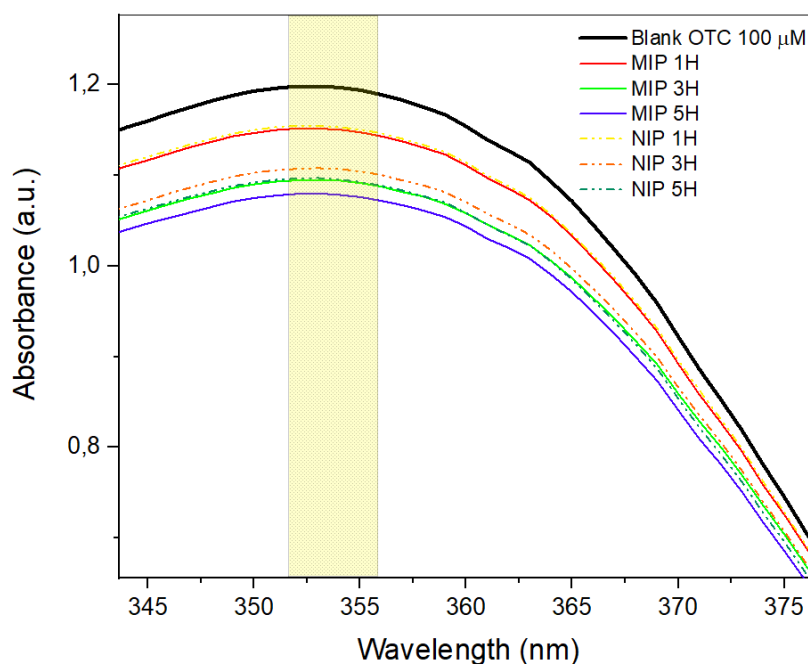


Fig. 41 Absorption spectra of DOT1 MIPs and NIPs incubated in rebinding solution 100 μM

Upon examining the absorption spectra, the signal of the MIPs is lower than the blank signal, as expected, indicating that they have captured a certain amount of the molecule of interest.

Despite the absence of complementary cavities for the template in NIPs, it is evident that even in these samples, the signal exhibits a decrease, due to the presence of non-

specific binding. However, the overall results show that MIPs captured more OTC than NIPs.

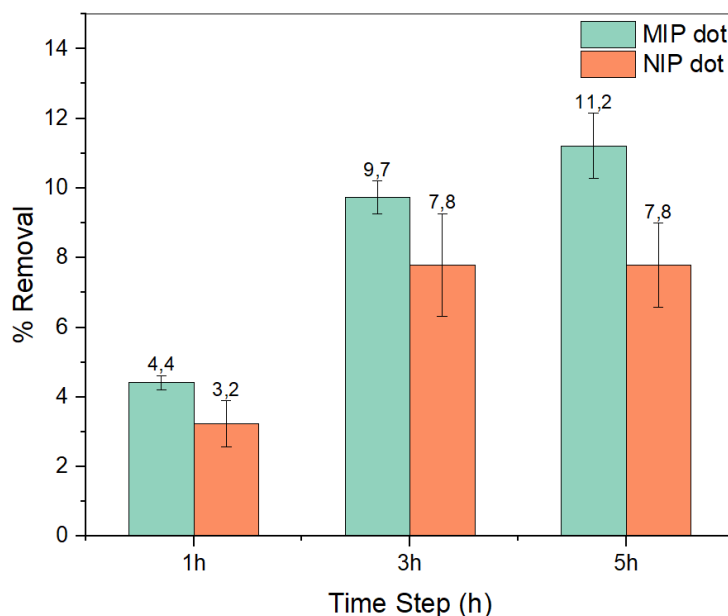


Fig. 42 %Removal of DOT1 MIP and NIP.

For statistical analysis, the chosen parameter was the percentage removal, the formula for which is detailed in Section 3.4.2. (Fig. 45). This parameter, calculated as described previously, allows for a comparison between the initial concentration of the antibiotic and the concentration remaining in the solution at each time point. This indirect measurement provides a precise numerical indication of the amount of the molecule captured by the tested samples.

Furthermore, a comparison of the percentage removal indicates that the performance of MIPs exceeds that of NIPs.

4.4.4. Second experiment, DOT2: MIP and NIP

In this second experiment, other six samples, three MIPs and three NIPs, were incubated into blank solutions with molarity 100 μM for different time steps, extending the experiment from 5h to 24h.

The decision to extend the experiment was driven by the necessity to verify the stability and repeatability of the results over a longer period. Additionally, we considered the necessity of assessing whether, over an extended period, the binding between the

cavities in the samples and the template would reach an equilibrium state or a stationary condition, which was not achieved within the initial 5-hour timeframe.

It is evident that the signal decreases at each time step, indicating antibiotic capture by the samples. Both MIPs and NIPs exhibit a decline in signal due to the presence of non-specific binding.

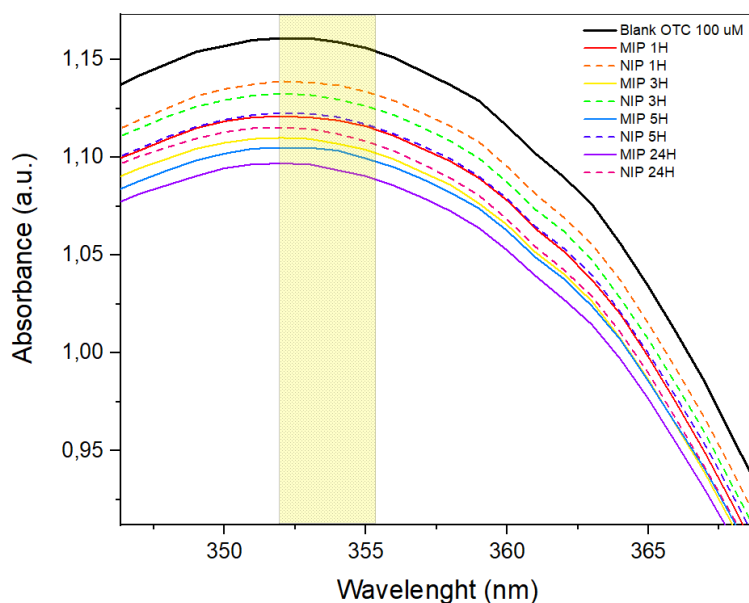


Fig. 43 Absorption spectra of DOT2 MIPs and NIPs incubated in rebinding solution 100 μ M

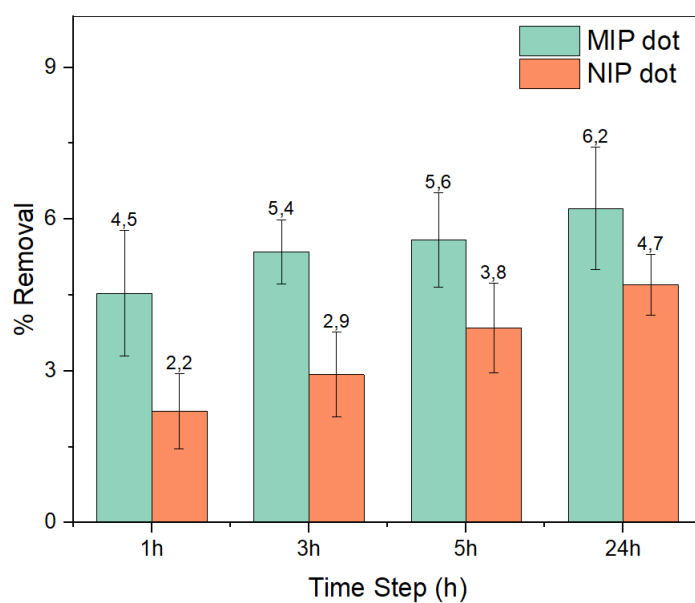


Fig. 44 %Removal of DOT2 MIP and NIP.

Once more, it can be observed (Fig.47) that the removal percentage for MIPs is higher than for NIPs at each time step, consistent with the previous experiment. However, the removal percentage values are lower than those in the DOT1 experiment. This discrepancy could be due to minor variations in the formulation or printing processes. Additionally, it should be noted that all absorbance measurements are highly dependent on the operator, as they involve pipetting operations when preparing the solution for analysis, introducing another variable that could affect the results.

4.4.5. Third experiment, DOT3: MIP and NIP

After the initial experiments were successfully completed, an additional test was conducted, altering the temperature at which the samples were maintained in the incubator. The temperature was adjusted to 37°C. This condition was modified because the increase in temperature enhances the agitation of the molecules in solution. The objective was to investigate how this increase in temperature could potentially improve or worsen the removal rate of the samples.

Due to the increase in temperature, the experimental setup required slight modifications. Instead of incubating the samples in a multi-well plate, each sample was placed in a small vial sealed with parafilm. This adjustment was made to prevent even minimal evaporation of the aqueous-based rebinding solution, considering the extended time steps characteristic of the experiment.

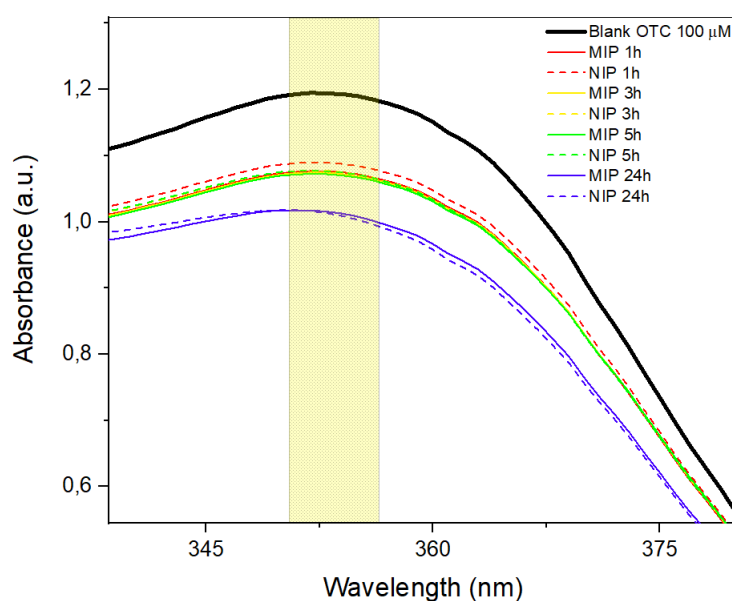


Fig. 45 Absorption spectra of DOT3 MIPs and NIPs incubated in rebinding solution 100 μM.

An interesting observation from these three experiments is that, in the third experiment, higher removal rates are achieved in a shorter period (*Fig.49*). After this initial increase, the rate remains relatively constant for the subsequent time-steps, suggesting a possible saturation of the OTC-selective binding sites. From 3 –hours on the percentage removal becomes very similar to that of the control samples, which may indicate a predominance of non-specific binding in both types of samples.

In this case it can be argued that a temperature increase may move the equilibrium between specifically bonded and a-specifically bonded and released molecules can be shifted towards lower specific absorption. Nevertheless, is interesting to observe that in the first stages of the experiment specificity seem saved, suggesting an acceleration of the binding reaction.

In conclusion, the results obtained by these tests do not appear univocal and further attempts will be necessary to better elucidate the influence of temperature in these rebinding experiments.

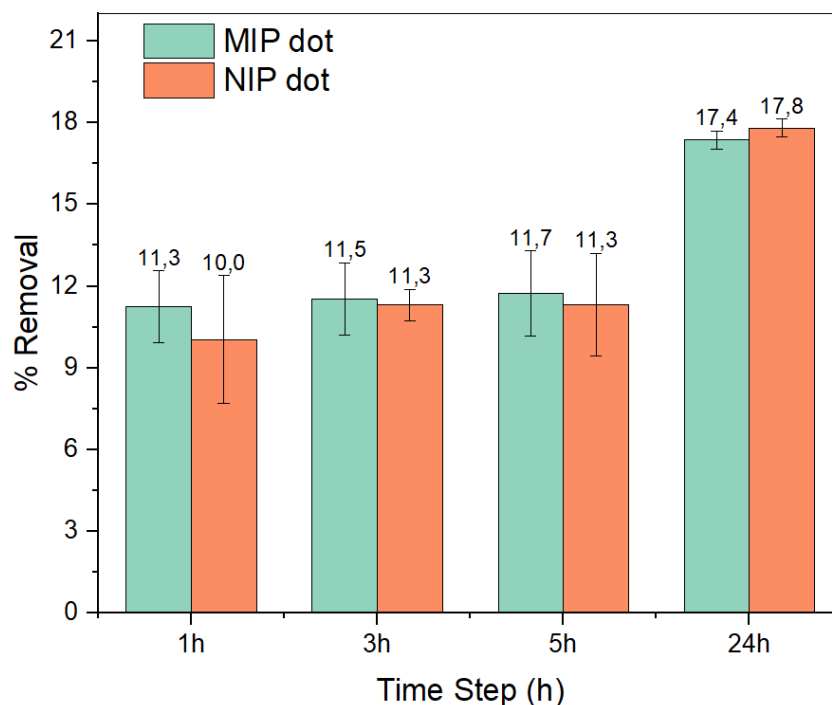


Fig. 46 %Removal of DOT3 MIP and NIP.

4.4.6. Fourth and fifth experiment: gyroids 1 MIP and gyroids 2 MIP

After testing the samples with the initial geometry, the experiment was conducted on gyroids. Two separate experiments were conducted under the same conditions as the DOT 3 experiment:

- The first experiment (gyroids 1 MIP) involved three MIP gyroid samples, incubated in three different wells within the rebinding solution.
- The second experiment (gyroids 2 MIP) involved six MIP gyroid samples, incubated in six different wells within the rebinding solution.

This experiment was repeated to investigate the repeatability of previous experiments and to ensure that the results obtained are reliable and not merely due to random errors or specific conditions present during a single execution. By increasing the number of samples, it was possible to evaluate variations in behaviour from sample to sample more closely.

The absorbance spectra for the MIP 1 and MIP 2 gyroids are presented individually. It can be observed from the graph (*Fig.50, Fig.51*) that, in those cases as well, the signal at the peak decreases over time.

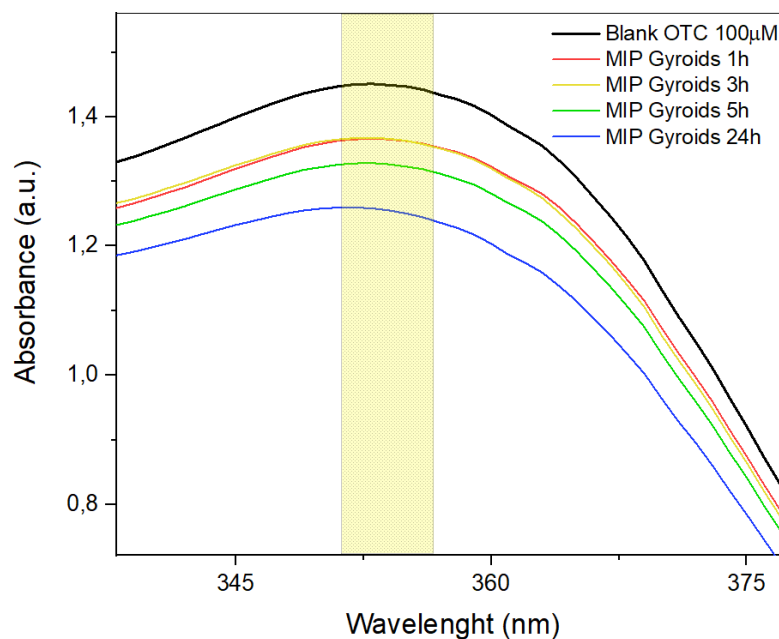


Fig. 47 Absorption spectra of MIP 1 Gyroids incubated in rebinding solution.

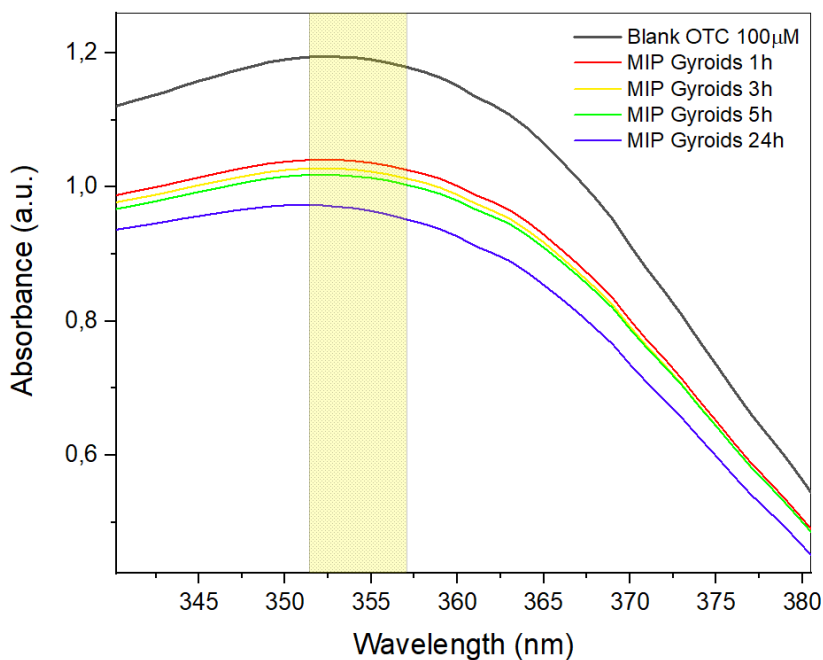


Fig. 48 Absorption spectra of MIP 2 Gyroids incubated in rebinding solution.

As evidenced by the results depicted in Figure 52, the percentage removal varies between the two experiments. Specifically, the first experiment achieved a removal rate of 15.6% at 24 hours, whereas the second experiment attained a removal rate of

25.3%. This indicates that the second experiment achieved an additional 9.7% removal compared to the first experiment.

Although the standard deviations within each experiment are acceptable and suggest robust results, there are noticeable differences between experiments repeated under the same conditions for both Dot MIPs and Gyroid MIPs. This indicates that the experiment's reliability is not optimal and requires further investigation.

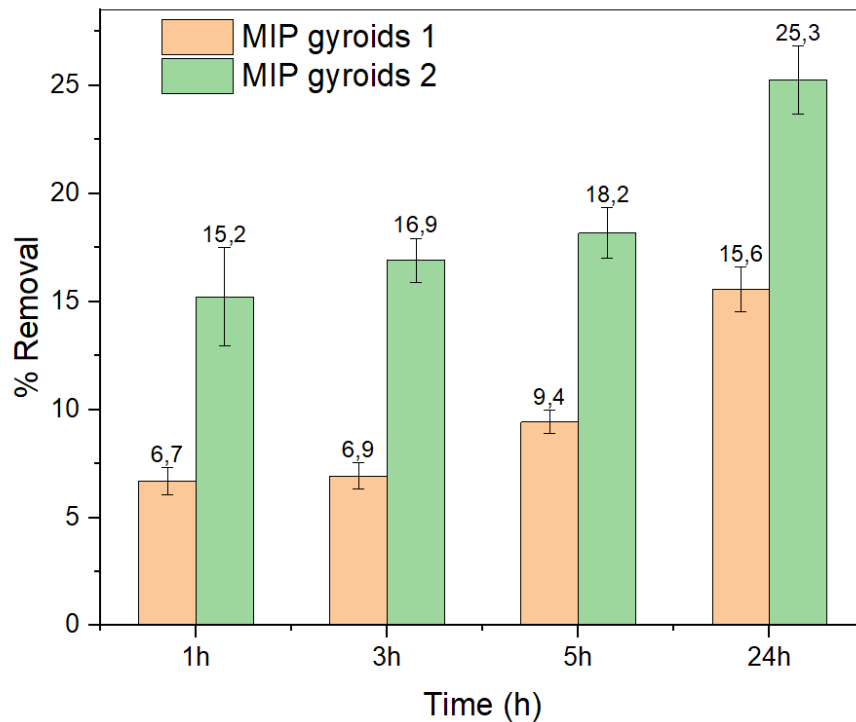


Fig. 49 %Removal of MIP 1(first experiment) and MIP 2 (second experiment) gyroids.

Regarding the removal percentages (Fig.52), significantly higher values were obtained compared to those achieved in experiments with the initial geometry.

The removal efficiency (Fig.52) shows a marked improvement, increasing from a maximum of 11% achieved in 5 hours for the Dot1 MIP to 18% for the gyroid 2 MIP.

In comparison to the Dot2 MIPs, that exhibited a removal efficiency of 6.7% over 24 hours (Fig. 49), the samples with gyroid geometry demonstrated significant enhancement, achieving removal efficiencies of 25.3% in 24 hours.

This could be attributed to the geometry variation: unlike the bulk geometry, the gyroids present a different exposed surface area available for binding with the template.

4.4.7. Sixth experiment: comparison of different surface area on MIP gyroids

The most recent experiment was also conducted on gyroids, but under different conditions. The objective was to compare the %removal of a single sample immersed in a volume of 750 μ L with that of two samples immersed in the same volume. This comparison was undertaken to evaluate how an increased surface area available for OTC binding influenced the removal percentage.

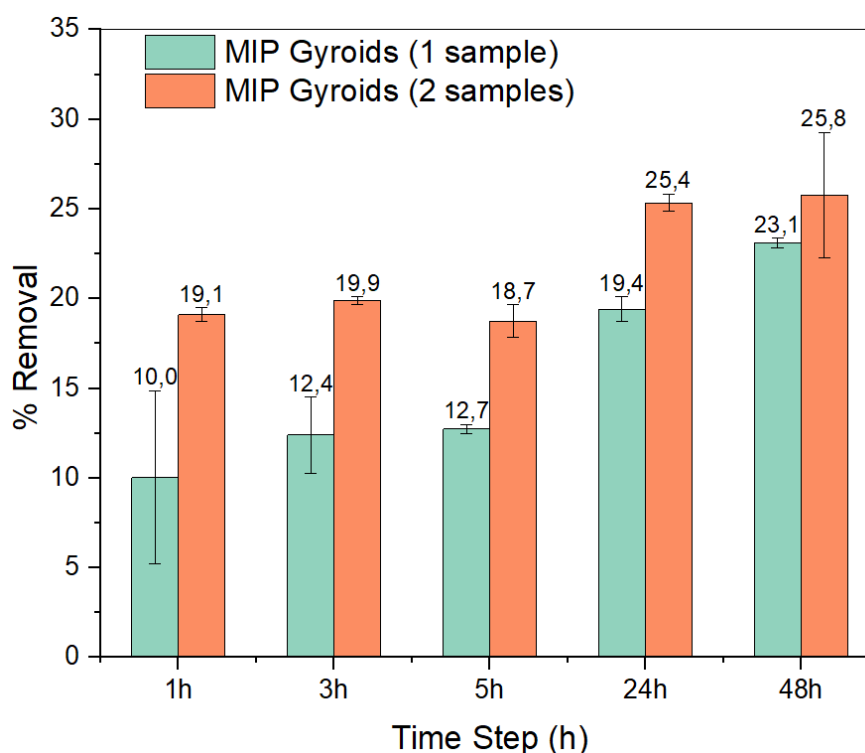


Fig. 50 % Removal of MIP Gyroids (comparison between 1 sample and 2 samples).

The results indicate that increasing the number of samples in the same volume, thereby expanding the available surface area for binding, leads to higher removal percentages of OTC at each time step. The standard deviations are relatively small, except for the 1-hour time step, indicating good precision and reliability of the measurements. The data underscores the significant impact of surface area on the effectiveness of the MIP gyroids in removing OTC from the solution. However, the increase in the removal rate between one sample and two samples is not linear,

suggesting that the samples may not have an equal number of available binding sites and may become saturated at different rates.

4.5. Washing After Rebinding (WAR)

In the final section of the results chapter, the absorbance spectra obtained after an additional washing step, performed following the rebinding step and referred to as "washing after rebinding," are presented. The spectra for the washed Dot 2 samples (Fig.54) and the gyroids (Fig. 55) from experiments comparing different surface areas are included.

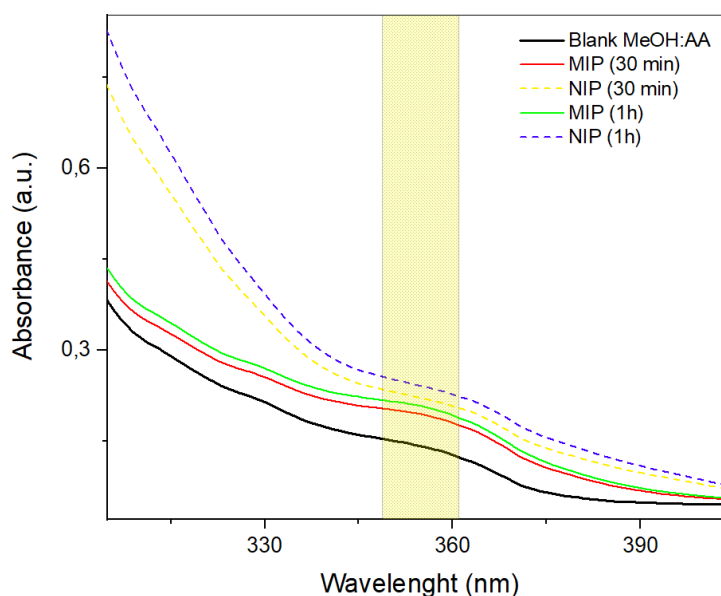


Fig. 51 WAR spectra of DOT 2 MIP and NIP.

In both experiments, it is evident that, compared to the control, antibiotic release from the samples occurs again.

Regarding the release from the Dot samples (Fig. 54), it is evident that, under the same washing conditions, the NIPs release more than the MIPs. This result may be attributed to the fact that the nonspecific interactions in the non-imprinted polymers are weaker compared to the binding that occurs when the antibiotic is captured in the selective pockets of the MIPs. For the gyroids (Fig.55), samples with a larger surface area, which bind a higher percentage of OTC during the rebinding step, also release a greater

amount during the second wash step. However, it is important to note that this relationship is not linear.

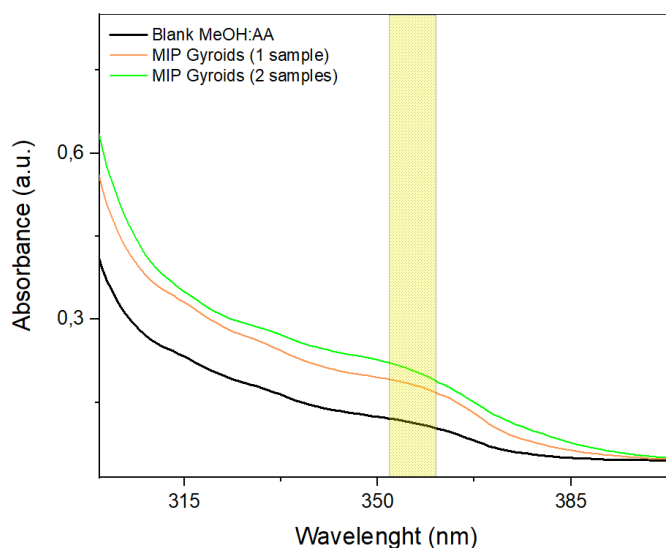


Fig. 52 WAR spectra of gyroids MIP (1 and 2 samples).

This experiment was conducted to assess the potential reuse of the MIP samples, leveraging the advantages outlined in the preceding chapter. Despite observing a secondary release of the antibiotic in all samples, notable irreversible surface breakage and modification were evident, particularly in the straightforward Dot geometry as depicted in Figure 56. In contrast, the gyroid geometry showed considerably less compromise. One possible contributor to the damage of the polymer matrix is the alternating immersion in relatively harsh solvents, such as the washing solution, and in water, such as the rebinding solution. Consequently, further investigations about the reuse of these devices are necessary, focusing preferably on complex geometries rather than thin and fragile ones.

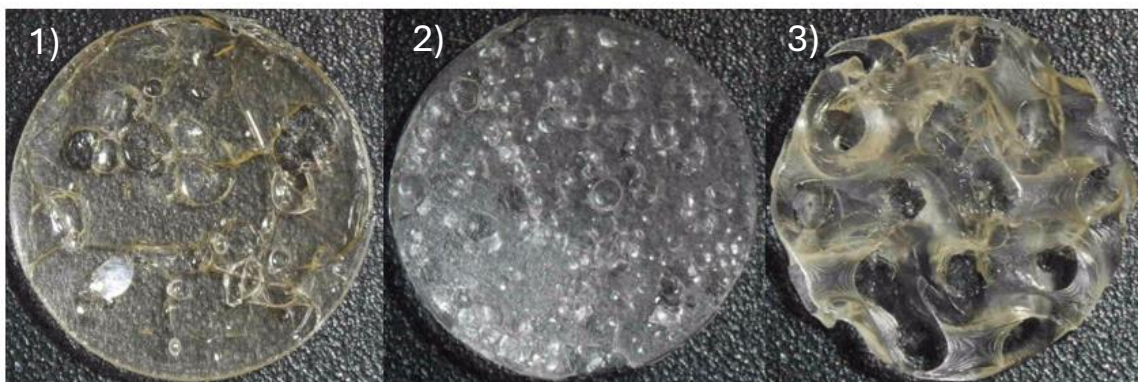


Fig. 53 MIP dot (1), NIP dot (2) and gyroid (3) samples washed after the rebinding procedure.

5. Conclusions and future work

The objective of this thesis was to fabricate Molecularly Imprinted Polymers (MIPs), which are synthetic receptors that mimic the natural molecular recognition mechanism of biological receptor molecules and can detect targets previously imprinted. The manufacturing technique chosen for the MIP samples in this thesis is DLP 3D printing, an additive manufacturing method. This relatively novel technique for MIP production enables fast, efficient, and scalable fabrication.

The MIPs were printed in two different geometries, and for each, a meticulous print optimization was conducted to obtain correctly printed samples with high resolution. Once printed, the ability of the materials to perform as MIPs was assessed by evaluating their capacity to capture the target molecule used during the imprinting procedure. This evaluation was performed using the batch rebinding method and analysed via UV-Vis spectroscopy.

The gyroid geometry yielded the best results in terms of both print quality and percentage of antibiotic removal, as discussed in the previous chapter. However, there were critical issues regarding the repeatability of the experiments, which warrant further investigation. Understanding the causes of these discrepancies and identifying the specific steps in the experimental process where variability is introduced is essential.

To advance this thesis project and achieve better results, future work could include the following:

- *Increase the statistics:* Conduct further repetitions of the experiments carried out during this thesis to improve the reliability of the obtained results.
- *Ingredient Testing:* Test other ingredients for the preparation of formulations and investigate their long-term toxicity, biodegradability, and biocompatibility.
- *Automation and Standardization:* Develop a technique to automate and standardize the washing procedure. This step is highly operator-dependent and

could lead to variations in the polymer matrix at the end of the washing process, resulting in significant variability in the results.

- *Selectivity Tests:* Perform selectivity tests to assess the specificity of the MIPs by rebinding in solutions containing different target molecules. This is to confirm that the rebinding of the previously imprinted molecule is greater than that of other molecules that form non-specific bonds with the samples.
- *Microfluidic Applications:* Consider practical applications in microfluidic contexts, given the geometry of the gyroids, which may allow for fluid flow through them. Exploring the integration of 3D-printed MIPs into existing water treatment infrastructures could extend the potential applications.

In conclusion, the results obtained in this thesis indicate that these synthetic receptors are particularly promising for filtration applications. Therefore, it would be advisable to conduct future studies to further investigate the role of fabrication in the efficiency of the finished material.

Bibliography

- [1] W. Cai and R. B. Gupta, "Molecularly-imprinted polymers selective for tetracycline binding," *Sep Purif Technol*, vol. 35, no. 3, pp. 215–221, Mar. 2004, doi: 10.1016/S1383-5866(03)00143-6.
- [2] J. Ashley, X. T. Feng, and Y. Sun, "A multifunctional molecularly imprinted polymer-based biosensor for direct detection of doxycycline in food samples," *Talanta*, vol. 182, pp. 49–54, May 2018, doi: 10.1016/j.talanta.2018.01.056.
- [3] E. Kaale, M. Chambuso, and J. Kitwala, "Analysis of residual oxytetracycline in fresh milk using polymer reversed-phase column," *Food Chem*, vol. 107, no. 3, pp. 1289–1293, Apr. 2008, doi: 10.1016/j.foodchem.2007.08.075.
- [4] M. SHARMA, "TOXIC EFFECT OF PHARMACEUTICALS WITH REFERENCE TO OXYTETRACYCLINE," *Asian Journal of Pharmaceutical and Clinical Research*, pp. 64–68, Jan. 2021, doi: 10.22159/ajpcr.2021.v14i1.39907.
- [5] K. A. Sarpong, W. Xu, W. Huang, and W. Yang, "The Development of Molecularly Imprinted Polymers in the Clean-Up of Water Pollutants: A Review," *Am J Analyt Chem*, vol. 10, no. 05, pp. 202–226, 2019, doi: 10.4236/ajac.2019.105017.
- [6] M. A. Zulfikar, D. Wahyuningrum, R. R. Mukti, and H. Setiyanto, "Molecularly imprinted polymers (MIPs): a functional material for removal of humic acid from peat water," *Desalination Water Treat*, vol. 57, no. 32, pp. 15164–15175, Jul. 2016, doi: 10.1080/19443994.2015.1069218.
- [7] C. Alexander, L. Davidson, and W. Hayes, "Imprinted polymers: Artificial molecular recognition materials with applications in synthesis and catalysis," Mar. 17, 2003, *Elsevier Ltd*. doi: 10.1016/S0040-4020(03)00152-2.
- [8] C. Alexander *et al.*, "Molecular imprinting science and technology: A survey of the literature for the years up to and including 2003," Mar. 2006. doi: 10.1002/jmr.760.
- [9] M. Marć and P. P. Wieczorek, "Introduction to MIP synthesis, characteristics and analytical application," in *Comprehensive Analytical Chemistry*, vol. 86, Elsevier B.V., 2019, pp. 1–15. doi: 10.1016/bs.coac.2019.05.010.
- [10] J. J. Belbruno, "Molecularly Imprinted Polymers," Jan. 09, 2019, *American Chemical Society*. doi: 10.1021/acs.chemrev.8b00171.
- [11] M. Włoch and J. Datta, "Synthesis and polymerisation techniques of molecularly imprinted polymers," in *Comprehensive Analytical Chemistry*, vol. 86, Elsevier B.V., 2019, pp. 17–40. doi: 10.1016/bs.coac.2019.05.011.
- [12] "A_historical_perspective_of_the_developm".
- [13] C. C. Villa, L. T. Sánchez, G. A. Valencia, S. Ahmed, and T. J. Gutiérrez, "Molecularly imprinted polymers for food applications: A review," May 01, 2021, *Elsevier Ltd*. doi: 10.1016/j.tifs.2021.03.003.
- [14] G. Vasapollo *et al.*, "Molecularly imprinted polymers: Present and future prospective," Sep. 2011. doi: 10.3390/ijms12095908.

- [15] F. Puoci, G. Cirillo, M. Curcio, O. I. Parisi, F. Iemma, and N. Picci, "Molecularly imprinted polymers in drug delivery: State of art and future perspectives," Oct. 2011. doi: 10.1517/17425247.2011.609166.
- [16] J. D. Marty and M. Mauzac, "Molecular imprinting: State of the art and perspectives," 2005. doi: 10.1007/b97573.
- [17] H. Kim and D. A. Spivak, "New insight into modeling non-covalently imprinted polymers," *J Am Chem Soc*, vol. 125, no. 37, pp. 11269–11275, Sep. 2003, doi: 10.1021/ja0361502.
- [18] "https://www.chimica-online.it/download/principio-le-chatelier.htm."
- [19] T. Sajini and B. Mathew, "A brief overview of molecularly imprinted polymers: Highlighting computational design, nano and photo-responsive imprinting," Dec. 01, 2021, *Elsevier B.V.* doi: 10.1016/j.talo.2021.100072.
- [20] G. Wulff, "REVIEWS Molecular Imprinting in Cross-Linked Materials with the Aid of Molecular Templates-A Way towards Artificial Antibodies."
- [21] Q. Wang, G.-Q. Wang, Y.-H. Fan, L. Zhang, and X.-Q. Yu, "Synthesis and copolymerization of pentachlorophenyl acrylate monomers".
- [22] "I P F 6."
- [23] S. Beyazit, B. Tse Sum Bui, K. Haupt, and C. Gonzato, "Molecularly imprinted polymer nanomaterials and nanocomposites by controlled/living radical polymerization," Nov. 01, 2016, *Elsevier Ltd.* doi: 10.1016/j.progpolymsci.2016.04.001.
- [24] A. Speltini, A. Scalabrini, F. Maraschi, M. Sturini, and A. Profumo, "Newest applications of molecularly imprinted polymers for extraction of contaminants from environmental and food matrices: A review," Jun. 29, 2017, *Elsevier B.V.* doi: 10.1016/j.aca.2017.04.042.
- [25] W. Derz, M. Fleischmann, and P. W. Elsinghorst, "Guiding molecularly imprinted polymer design by pharmacophore modeling," *Molecules*, vol. 26, no. 16, Aug. 2021, doi: 10.3390/molecules26165101.
- [26] C. M. Dai, X. F. Zhou, Y. L. Zhang, S. G. Liu, and J. Zhang, "Synthesis by precipitation polymerization of molecularly imprinted polymer for the selective extraction of diclofenac from water samples," *J Hazard Mater*, vol. 198, pp. 175–181, Dec. 2011, doi: 10.1016/j.jhazmat.2011.10.027.
- [27] Y. Yang and X. Shen, "Preparation and Application of Molecularly Imprinted Polymers for Flavonoids: Review and Perspective," Nov. 01, 2022, *MDPI*. doi: 10.3390/molecules27217355.
- [28] K. Kwaśniewska, R. Gadzała-Kopciuch, and B. Buszewski, "Magnetic molecular imprinted polymers as a tool for isolation and purification of biological samples," *Open Chem*, vol. 13, no. 1, pp. 1228–1235, 2015, doi: 10.1515/chem-2015-0137.
- [29] L. Piscopo *et al.*, "Uniformly Sized Molecularly Imprinted Polymers (MIPs) for 17 β -Estradiol."
- [30] A. Lamaoui, V. Mani, C. Durmus, K. N. Salama, and A. Amine, "Molecularly imprinted polymers: A closer look at the template removal and analyte binding," Jan. 01, 2024, *Elsevier Ltd.* doi: 10.1016/j.bios.2023.115774.

- [31] R. A. Lorenzo, A. M. Carro, C. Alvarez-Lorenzo, and A. Concheiro, "To remove or not to remove? The challenge of extracting the template to make the cavities available in molecularly imprinted polymers (MIPs)," Jul. 2011. doi: 10.3390/ijms12074327.
- [32] Carmen Alvarez-Lorenzo and Angel Concheiro, *Handbook of Molecularly Imprinted Polymers*. 2013.
- [33] M. D. Luque de Castro and F. Priego-Capote, "Soxhlet extraction: Past and present panacea," Apr. 2010. doi: 10.1016/j.chroma.2009.11.027.
- [34] "Microwaves <https://www.chimica-online.it/download/microonde.htm>."
- [35] C. R. T. Tarley, A. M. Basaglia, M. G. Segatelli, M. C. Prete, F. A. C. Suquila, and L. L. G. de Oliveira, "Preparation and application of nanocomposite based on imprinted poly(methacrylic acid)-PAN/MWCNT as a new electrochemical selective sensing platform of Pb²⁺ in water samples," *Journal of Electroanalytical Chemistry*, vol. 801, pp. 114–121, Sep. 2017, doi: 10.1016/j.jelechem.2017.07.033.
- [36] L. Samandari, A. Bahrami, M. Shamsipur, L. Farzin, and B. Hashemi, "Electrochemical preconcentration of ultra-trace Cd²⁺ from environmental and biological samples prior to its determination using carbon paste electrode impregnated with ion imprinted polymer nanoparticles," *Int J Environ Anal Chem*, vol. 99, no. 2, pp. 172–186, Jan. 2019, doi: 10.1080/03067319.2019.1583334.
- [37] T. Cowen and M. Cheffena, "Template Imprinting Versus Porogen Imprinting of Small Molecules: A Review of Molecularly Imprinted Polymers in Gas Sensing," Sep. 01, 2022, *MDPI*. doi: 10.3390/ijms23179642.
- [38] X. He, L. Zang, Y. Xin, and Y. Zou, "An overview of photopolymerization and its diverse applications," Dec. 01, 2023, *John Wiley and Sons Inc*. doi: 10.1002/appl.202300030.
- [39] H. B. Sun and S. Kawata, "Two-photon photopolymerization and 3D lithographic microfabrication," 2004. doi: 10.1007/b94405.
- [40] "<https://specificpolymers.com/innovation-in-photopolymerization-toward-innovative-materials-and-coatings/>."
- [41] "Difference between CNC and 3D printing <https://www.roboze.com/en/resources/difference-between-3d-printing-and-cnc-machining.html>."
- [42] S. Saleh Alghamdi, S. John, N. Roy Choudhury, and N. K. Dutta, "polymers Additive Manufacturing of Polymer Materials: Progress, Promise and Challenges," 2021, doi: 10.3390/polym13.
- [43] B. Ahuja, M. Karg, and M. Schmidt, "Additive manufacturing in production: challenges and opportunities," in *Laser 3D Manufacturing II*, SPIE, Mar. 2015, p. 935304. doi: 10.1117/12.2082521.
- [44] S. A. M. Tofail, E. P. Koumoulos, A. Bandyopadhyay, S. Bose, L. O'Donoghue, and C. Charitidis, "Additive manufacturing: scientific and technological challenges, market uptake and opportunities," Jan. 01, 2018, *Elsevier B.V*. doi: 10.1016/j.mattod.2017.07.001.
- [45] "Workflow of 3D Printing Process <https://www.theengineeringprojects.com/2021/06/what-is-3d-printing-definition-technology-and-applications.html>."

- [46] S. Dufera Tolcha, K. Srinivasulu Reddy, and S. Dufera, "10 - IJMITE - Additive Manufacturing," 2019. [Online]. Available: <https://www.researchgate.net/publication/334545466>
- [47] M. Layani, X. Wang, and S. Magdassi, "Novel Materials for 3D Printing by Photopolymerization," Oct. 11, 2018, *Wiley-VCH Verlag*. doi: 10.1002/adma.201706344.
- [48] K. L. Sampson *et al.*, "Multimaterial Vat Polymerization Additive Manufacturing," Sep. 10, 2021, *American Chemical Society*. doi: 10.1021/acsapm.1c00262.
- [49] M. Sirbubalo, A. Tucak, K. Muhamedagić, O. Rahić, A. Čekić, and E. Vranić, "Photopolymerization-Based Technologies for Microneedle Arrays Production," in *IFMBE Proceedings*, Springer Science and Business Media Deutschland GmbH, 2021, pp. 670–678. doi: 10.1007/978-3-030-73909-6_77.
- [50] "The Difference between DLP and SLA 3D Printing Technology <https://manufactur3dmag.com/difference-dlp-sla/>."
- [51] R. Rezanavaz, M. Petcu, M. J. Le Guen, and A. Dubois, "Three-Dimensional Printing of Molecularly Imprinted Polymers by Digital Light Processing for Copper Ion Sequestration," *3D Print Addit Manuf*, vol. 11, no. 2, pp. E619–E627, Apr. 2024, doi: 10.1089/3dp.2022.0107.
- [52] P. G. Conrad *et al.*, "Functional molecularly imprinted polymer microstructures fabricated using microstereolithography," *Advanced Materials*, vol. 15, no. 18, pp. 1541–1544, Sep. 2003, doi: 10.1002/adma.200304602.
- [53] L. P. C. Gomez *et al.*, "Rapid Prototyping of Chemical Microsensors Based on Molecularly Imprinted Polymers Synthesized by Two-Photon Stereolithography," *Advanced Materials*, vol. 28, no. 28, pp. 5931–5937, Jul. 2016, doi: 10.1002/adma.201600218.
- [54] Spangenberg A, Chia GL, Malval JP, and et al., "Preparation of molecularly imprinted polymers by two-photon stereolithography.," *Google Patents; 2017.*
- [55] »»"?£ :S, "NATIONAL TOXICOLOGY PROGRAM Technical Report Series No. 315 IN F344/N RATS AND B6C3Fi MICE (FEED STUDIES)."
- [56] H. Yan and K. Ho Row, "Characteristic and Synthetic Approach of Molecularly Imprinted Polymer," *Int. J. Mol. Sci*, vol. 7, pp. 155–178, 2006, [Online]. Available: www.mdpi.org/ijms/
- [57] "Compound summary: Methacrylic Acid [https://pubchem.ncbi.nlm.nih.gov/compound/Methacrylic-Acid.](https://pubchem.ncbi.nlm.nih.gov/compound/Methacrylic-Acid/)"
- [58] "DPGDA - allnex. Allnex. [https://allnex.com/en/product/82a3a083-2bdd-46a5-abcc11eb48f59dfd/dpgda.](https://allnex.com/en/product/82a3a083-2bdd-46a5-abcc11eb48f59dfd/dpgda/)"
- [59] "DMSO [https://www.gaylordchemical.com/products/literature/physical-properties/.](https://www.gaylordchemical.com/products/literature/physical-properties/)"
- [60] "Guidechem chemical B2B network provides information on china and global chemical market quotation and relative chemical Information.Guidechem Chemical Network providing the most complete information of the chemical industry. GuideChem. [https://www.guidechem.com/.](https://www.guidechem.com/)"
- [61] M. Dossot, H. Obeid, X. Allonas, P. Jacques, J. P. Fouassier, and A. Merlin, "Photopolymerization of Acrylates in the Presence of Phenolic Derivatives: Role of the Photoinitiating System," 2004.

- [62] “<https://www.sigmaaldrich.com/IT/it/product/aldrich/511447>.”
- [63] “<https://www.asiga.com/max-x/>.”
- [64] “Asiga® Flash Cure Box. <https://www.stuller.com/products/24-1110/?groupId=211901&categoryId=25130&recommendationSource=CategoryBrowse&recommendationIndex=21>.”
- [65] “rheology and photoreology <https://wiki.anton-paar.com/en/basics-of-rheology/>.”
- [66] H.-H. Perkampus, *UV-VIS Spectroscopy and Its Applications*. Springer Berlin Heidelberg, 1992. doi: 10.1007/978-3-642-77477-5.
- [67] “Spettroscopia UV-visibile (parte 1).”
- [68] M. H. Penner, “Basic Principles of Spectroscopy,” 2017, pp. 79–88. doi: 10.1007/978-3-319-45776-5_6.
- [69] “<https://www.biospx.com/product/synergy-htx/>.”
- [70] “R-squared value <https://www.flowinjection.com/app-notes/the-coefficient-of-determination-vs-relative-standard-error>.”
- [71] “https://www.mt.com/it/it/home/applications/L1_AutoChem_Applications/ftir-spectroscopy/attenuated-total-reflectance-atr.html.”
- [72] H. Tiernan, B. Byrne, and S. G. Kazarian, “ATR-FTIR spectroscopy and spectroscopic imaging for the analysis of biopharmaceuticals,” Nov. 05, 2020, *Elsevier B.V.* doi: 10.1016/j.saa.2020.118636.
- [73] Feng Y and Roos WH, “Atomic Force Microscopy: An Introduction. *Methods Mol Biol.* 2024;2694:295-316. doi: 10.1007/978-1-0716-3377-9_14. PMID: 37824010.”.
- [74] F. Xia and K. Youcef-Toumi, “Review: Advanced Atomic Force Microscopy Modes for Biomedical Research,” Dec. 01, 2022, *MDPI*. doi: 10.3390/bios12121116.
- [75] “<https://www.3shape.com/it/scanners/e-series>.”
- [76] M. Gastaldi *et al.*, “Functional Dyes in Polymeric 3D Printing: Applications and Perspectives,” Jan. 04, 2021, *American Chemical Society*. doi: 10.1021/acsmaterialslett.0c00455.